Original Article

MOLECULAR METABOLISM

Hepatic sialic acid synthesis modulates glucose homeostasis in both liver and skeletal muscle

Jun Peng [1,**], Liming Yu [1,8], Linzhang Huang [1,9], Vivian A. Paschoal [2], Haiyan Chu [1,10], Camila O. de Souza [2], Joseph V. Varre [3], Da Young Oh [2], Jennifer J. Kohler [4], Xue Xiao [5], Lin Xu [5], William L. Holland [3], Philip W. Shaul [1,*,7], Chieko Mineo [1,6,***,7]

ABSTRACT

Objective: Sialic acid is a terminal monosaccharide of glycans in glycoproteins and glycolipids, and its derivation from glucose is regulated by the rate-limiting enzyme UDP-GlcNAc 2-epimerase/ManNAc kinase (GNE). Although the glycans on key endogenous hepatic proteins governing glucose metabolism are sialylated, how sialic acid synthesis and sialylation in the liver influence glucose homeostasis is unknown. Studies were designed to fill this knowledge gap.

Methods: To decrease the production of sialic acid and sialylation in hepatocytes, a hepatocyte-specific GNE knockdown mouse model was generated, and systemic glucose metabolism, hepatic insulin signaling and glucagon signaling were evaluated in vivo or in primary hepatocytes. Peripheral insulin sensitivity was also assessed. Furthermore, the mechanisms by which sialylation in the liver influences hepatic insulin signaling and glucagon signaling and peripheral insulin sensitivity were identified.

Results: Liver GNE deletion in mice caused an impairment of insulin suppression of hepatic glucose production. This was due to a decrease in the sialylation of hepatic insulin receptors (IR) and a decline in IR abundance due to exaggerated degradation through the Eph receptor B4. Hepatic GNE deficiency also caused a blunting of hepatic glucagon receptor (GCGR) function which was related to a decline in its sialylation and affinity for glucagon. An accompanying upregulation of hepatic FGF21 production caused an enhancement of skeletal muscle glucose disposal that led to an overall increase in glucose tolerance and insulin sensitivity.

Conclusion: These collective observations reveal that hepatic sialic acid synthesis and sialylation modulate glucose homeostasis in both the liver and skeletal muscle. By interrogating how hepatic sialic acid synthesis influences glucose control mechanisms in the liver, a new metabolic cycle has been identified in which a key constituent of glycans generated from glucose modulates the systemic control of its precursor.

Keywords FGF21; Glucagon receptor; Glucose; GNE; Insulin receptor; Sialic acid

1. INTRODUCTION

Sialic acid is a terminal monosaccharide of glycans that are covalently linked with proteins or lipids to form glycoproteins and glycolipids. The terminal sialylation of glycoproteins influences diverse aspects of protein biology, including protein conformation and intracellular transport, and cell surface receptor signal transduction [1—3]. Glycolipids, which are primarily localized on the plasma membrane, play a structural role to maintain membrane stability, and they facilitate cell—cell communication acting as receptors, anchors for proteins and regulators of signal transduction [4]. The key enzyme in sialic acid production from glucose is the bifunctional UDP-N-acetylglucosamine-2-epimerase/N-acetylmannosamine kinase (GNE), which catalyzes two rate-limiting steps in sialic acid biosynthesis in the cytosol [5—7]. The global inactivation of GNE by gene targeting causes early embryonic lethality in mice, thereby emphasizing

[1]Center for Pulmonary and Vascular Biology, Dept. of Pediatrics, University of Texas Southwestern Medical Center, 5323 Harry Hines Blvd., Dallas, TX, 75390, USA [2]Dept. of Internal Medicine, University of Texas Southwestern Medical Center, 5323 Harry Hines Blvd., Dallas, TX, 75390, USA [3]Dept. of Nutrition & Integrative Physiology, University of Utah College of Health, 250 1850 E, Salt Lake City, UT, 84112, USA [4]Dept. of Biochemistry, University of Texas Southwestern Medical Center, 5323 Harry Hines Blvd., Dallas, TX, 75390, USA [5]Peter O'Donnell Jr. School of Public Health, University of Texas Southwestern Medical Center, 5323 Harry Hines Blvd., Dallas, TX, 75390, USA [6]Dept. of Cell Biology, University of Texas Southwestern Medical Center, 5323 Harry Hines Blvd., Dallas, TX, 75390, USA

[7] Philip W. Shaul and Chieko Mineo contributed equally to this work.
[8] Current address: Dept. of Pharmacology, UT Health San Antonio, 7703 Floyd Curl Drive, MC7764, San Antonio, TX, 78229, USA.
[9] Current address: Shanghai Key Laboratory of Metabolic Remodeling and Health, Fudan University, Shanghai, 200433, China.
[10] Current address: State Key Laboratory of Genetic Engineering, School of Life Sciences, Fudan University, Shanghai, China.

*Corresponding author. E-mail: philip.shaul@utsouthwestern.edu (P.W. Shaul).

***Corresponding author. Center for Pulmonary and Vascular Biology, Dept. of Pediatrics, University of Texas Southwestern Medical Center, 5323 Harry Hines Blvd., Dallas, TX, 75390, USA. E-mail: chieko.mineo@utsouthwestern.edu (C. Mineo).

**Corresponding author. E-mail: Jun.Peng@utsouthwestern.edu (J. Peng).

Received August 1, 2023 • Revision received September 22, 2023 • Accepted September 26, 2023 • Available online 28 September 2023

https://doi.org/10.1016/j.molmet.2023.101812

the fundamental role of the enzyme and sialylation during development [8].

With the notable exception of albumin, the majority of circulating proteins, which are primarily hepatic in origin, are glycosylated [9,10], indicating that this form of post-translational modification is prevalent in the liver. There are possible mechanistic links between hepatic sialic acid production and sialylation and glucose homeostasis because the glycans on key endogenous hepatic proteins governing glucose metabolism, including the insulin receptor (IR) and glucagon receptor (GCGR), are terminally sialylated [11–13]. Insulin action via hepatic IR decreases gluconeogenesis and glycogenolysis and it increases glycogenesis, and glucagon activation of hepatic GCGR promotes glycogenolysis and gluconeogenesis and attenuates glycogenesis [14,15]. The liver is also a key source of FGF21, which has a number of actions that increase glycemic control [16], and hepatocytes are a target of the effects of non-esterified fatty acids (NEFA) on glucose metabolism [17]. It is entirely unknown whether sialic acid synthesis and sialylation in the liver influence glucose homeostatic processes in hepatocytes.

To fill the knowledge gap about hepatic sialic acid production and sialylation and glucose control, in the present work we selectively deleted GNE from the liver postnatally in mice. The resulting decrease in hepatic sialic acid synthesis caused an impairment of insulin suppression of hepatic glucose production, a blunting of hepatic GCGR function, and an enhancement of skeletal muscle glucose disposal, with a composite positive impact on global glucose tolerance and insulin sensitivity. Additional experiments interrogated the underpinnings of the changes in liver insulin and glucagon action and the role of hepatocyte-derived FGF21 in the alterations in peripheral glucose disposal. Recognizing that sialic acid biosynthesis begins with glucose [1,18], the new findings reveal that there is a metabolic cycle comprised of glucose conversion to sialic acid and sialic acid influence on glucose homeostasis.

2. MATERIALS AND METHODS

2.1. Mouse models

Floxed GNE mice ($GNE^{fl/fl}$) were generated in which LoxP sites were inserted into intron 2 and intron 3 of the *Gne* gene using a CRISPR-Cas9-mediated genomic editing strategy as previously described [19]. Albumin-Cre mice (Stock No. 003574) were obtained from the Jackson Laboratory, and $FGF21^{fl/fl}$ mice were provided by Dr. Steven Kliewer (University of Texas Southwestern Medical Center). All mouse strains were on C57BL/6J background. The mice were housed in a specific pathogen-free, temperature- and humidity-controlled animal facility at 22 °C under a 12-h/12-h light/dark cycle. All the breeders and weaned pups were fed a standard chow diet. All animal experiments were conducted in accordance with policies of the NIH Guide for the Care and Use of Laboratory Animals, and they were approved by the Institutional Animal Care and Use Committee (IACUC) of the University of Texas Southwestern Medical Center (APN#2015-101173).

Male or female mice were fed a control diet (Research Diets; D12329, with 11% kcal from fat) or a high fat diet (Research Diets; D12331, with 58% kcal from fat) as indicated. For studies in lean mice, the mice were fed the control diet and intravenously (IV) injected at 5 weeks of age with 4×10^{11} genomic copies per mouse of adeno-associated-virus serotype 8 (AAV8) encoding thyroxine-binding globulin (TBG) promoter-driven Cre recombinase to generate liver specific knockout of GNE (GNE^{LKO}), FGF21 ($FGF21^{LKO}$) or both GNE and FGF21 (GNE^{L-KO};$FGF21^{LKO}$). Mice injected with AAV8-TBG expressing GFP instead of Cre recombinase served as controls and were designated as wild-type (WT) [20,21]. Experiments were performed two weeks following AAV8 injection. pAAV8-TBG-GFP (Addgene plasmid # 105535) and pAAV8-TBG-Cre (Addgene plasmid # 107787), gifts from James M. Wilson, were packaged into 293T cells by 3-plasmid transfection (Shuttle, Rep/Cap, pAdDeltaF6 helper), and the AAV were precipitated by PEG and purified by iodixanol density gradient at the Baylor College of Medicine Gene Vector Core. To generate mice with constitutive liver-specific GNE deletion, $GNE^{fl/fl}$ mice were crossed with Albumin-Cre mice. $GNE^{fl/fl}$;Albumin-Cre and their $GNE^{fl/fl}$ littermates were fed a control diet post-weaning and experiments were performed at 15 weeks of age. To evaluate the abundance and sialylation of the glucagon receptor (GCGR), a flag- and myc-tagged GCGR was expressed in the liver using AAV8-TBG-GCGR-Flag-Myc (Vector Builder). At 5 weeks of age $GNE^{fl/fl}$ mice were concurrently injected with 4×10^{11} genomic copies per mouse of AAV8-TBG-GFP and AAV8-TBG-GCGR-Flag-Myc, or AAV8-TBG-Cre and AAV8-TBG-GCGR-Flag-Myc. Two weeks following AAV8 injection, the livers were harvested for further study. To evaluate the effect of liver-specific GNE deletion on established HFD-induced insulin resistance, beginning at 5 weeks of age, male $GNE^{fl/fl}$ mice were fed with high-fat diet for 20 weeks and then injected with AAV8-TBG-GFP or AAV8-TBG-Cre, and experiments were performed 2 weeks later.

Body weight, fat mass and lean body mass were measured by NMR (Minispec NMR Analyzer, Bruker) in the afternoon, and body composition was expressed as the ratio of fat mass or lean mass to body weight. For fasting and refeeding experiments, mice were fasted for 16 h overnight and then euthanized (fasted group) or refed with control diet (Research Diets; D12329, with 11% kcal from fat) for an additional 4 h before euthanizing (refed group). To evaluate food consumption, mice were placed in a clean cage, the amount of food was weighed at 10:00 AM on three consecutive days, and the consumption was calculated in g/mouse/day.

Plasma insulin, glucagon, total GLP-1 and FGF21 were measured by ELISA (ALPCO, Crystal Chem, Crystal Chem and Abcam, respectively). Liver lipids were isolated using a chloroform-free method (Abcam) according to the manufacturer's instructions. Serum and liver triglycerides and cholesterol were measured by colorimetric and fluorometric methods (Thermo Scientific). Enzymatic colorimetric methods were used to quantify plasma and hepatic free fatty acids (FFA; FUJIFILM WAKO Chemicals), and plasma aspartate aminotransferase (AST) and alanine aminotransferase (ALT) activity (Sigma–Aldrich).

2.2. Glucose, insulin, glucagon and pyruvate tolerance tests (GTT, ITT, GcTT and PTT)

To initially interrogate glucose regulation, GTT and ITT were employed. In GTT the mice received an intraperitoneal (IP) injection of dextrose (1 g/kg B.W.) after 6 h of fasting (9 AM to 3 PM), and blood was drawn through tail-vein bleeding to measure glucose levels using a glucometer (Contour, Ascensia Diabetes Care US Inc) at 0, 15, 30, 60, 90, and 120 min after dextrose injection. For ITT, 0.5 units/kg B.W. of insulin (Humulin, Eli Lilly) was IP injected after 6 h of fasting, and blood was drawn at 0, 15, 45, 90, and 120 min after insulin injection. In GcTT, mice were IP injected with human glucagon (16 μg/kg B.W.) after 6 h of fasting, and blood was drawn to measure glucose levels at 0, 15, 30, 60, 90, and 120 min after glucagon injection. In PTT, pyruvate sodium (2 g/kg B.W.) was IP injected to mice with 16 h fasting (6 PM previous day to 10 AM), and blood was drawn to measure glucose levels at 0, 15, 30, 60, 90, and 120 min after the injection. For insulin secretion during GTT, blood was collected in a MicrovetteCB tube (SARSTEDT AG & Co. KG) with lithium heparin through tail-vein bleeding at the indicated time after dextrose injection.

2.3. Hyperinsulinemic—euglycemic clamps

Hyperinsulinemic—euglycemic clamp studies were performed using previously described methods [22,23]. Briefly, a catheter was surgically implanted in the right jugular vein and tunneled subcutaneously and exteriorized at the back of the neck. After three to five days of recovery, only mice losing less than 10% of their pre-cannulation weight were used. The clamp experiments began with a constant infusion (5 μCi/h) of D-[3-^{3}H] glucose (PerkinElmer) in 6-h-fasted mice. After 90 min of tracer equilibration and basal sampling, glucose (50% dextrose) and tracer (5 μCi/h) plus insulin (10 mU/kg/min, Humulin, Lilly) were infused into the jugular vein. Blood glucose was measured by glucose strip (Contour, Ascensia Diabetes Care US Inc) at 10 min intervals. The steady-state conditions (120 mg/dl ± 10 mg/dl) were confirmed at the end of the clamp by maintaining glucose infusion and blood glucose concentration for a minimum of 20 min. Blood samples at time points −10, 0 (basal), 110, and 120 min (end of experiment) were taken to determine glucose-specific activity, as well as free fatty acid and insulin concentration. At the end of the clamp period, the mice were euthanized and blood and tissue samples were obtained. Tracer-determined rates were quantified using the Steele equation for steady-state conditions. At steady state, the glucose disposal rate (GDR) is equal to the sum of the rate of endogenous hepatic glucose production (HGP) plus the exogenous glucose infusion rate (GIR). The insulin-stimulated GDR (IS-GDR) is equal to the total GDR minus the basal glucose turnover rate.

2.4. Insulin and glucagon signaling

To evaluate insulin signaling in the liver, mice fasted 6 h were IV injected with vehicle (saline) or insulin. Five minutes later, the liver was harvested and snap frozen in liquid nitrogen for later immunoblotting. Comparable methods were employed to evaluate insulin signaling in skeletal muscle. For glucagon receptor signaling in vivo, non-fasting mice (9:00 AM) were IP injected with 1 mg/kg human glucagon (Sigma) or vehicle saline, and liver tissue was collected 5 min later and snap frozen in liquid nitrogen. cAMP levels in the liver were measured by ELISA (Abcam) according to the manufacture's alternative lysis protocol. PKA activity was detected colorimetrically (ThermoFisher) and phospho-PKA substrates were evaluated by Western blot.

2.5. Liver glycogen and glycogenesis

Liver glycogen content was measured as previously described [24,25]. In brief, liver tissue was placed in 1 N KOH for 20 min at 55 °C, an aliquot of the alkaline extract (100 μL) was neutralized with 1 N HCl (100 μL), and its pH was adjusted to 4.9 with 0.15 N sodium acetate buffer (HAc-NaAc, pH 4.9, 200 μL). Then the acidified samples were divided into two aliquots and incubated with or without amylglucosidase (Sigma) for 1 h at 37 °C. The glucose concentration in the two aliquots was quantified using hexokinase-based glucose assays (ThermoFisher). The glycogen concentration was calculated by dividing the difference in the glucose concentration between the amyloglucosidase-treated and untreated samples by tissue weight.

Glycogenesis was determined by measuring [^{3}H] 2-deoxy-D-glucose (2-DOG) incorporation into liver glycogen during a GTT as previously described [24—26]. After fasting for 16 h mice were IP injected with 20% dextrose and 2-DOG (2 g/kg; 10 μCi/mouse; Amersham Radiolabeled Chemicals), and blood samples (15 μL) were collected into MicrovetteCB tubes (SARSTEDT AG & Co. KG) from the tail vein at 0, 10, 20, 30, 60, 90 and 120 min, after which the mice were euthanized and the tissues of interest were snap frozen in liquid nitrogen. To determine the 2-DOG-specific activity in plasma, 3 μL of plasma was deproteinized with 200 μL 0.55 M ice-cold perchloric acid (PCA) and centrifuged. 180 μL of supernatant was neutralized with 45 μL of 2.2 M $KHCO_3$, and radioactivity was then measured in a scintillation counter. The glucose-specific activity (GSA, degenerations/min/μg) was calculated by dividing the radioactivity by the blood glucose concentration, and the area under the curve (AUC) was integrated for the duration of the experiment. To assess 2-DOG incorporation into glycogen, frozen liver (60 mg) was homogenized in 500 μL 1 N KOH and then digested for 20 min at 55 °C. Once dissolved, the extracts were chilled on ice. One aliquot was used to measure the total glycogen concentration as described above. A second 350 μL aliquot was added to 700 μL of prechilled 100% ethanol, and macromolecule precipitation was performed for 2 h at −20 °C and followed by centrifugation at 4000 × *g* for 20 min at 4 °C. After being washed three times with 66% ethanol (−20 °C), the pellet was allowed to dry and later dissolved in 100 μL of 1 N KOH for 20 min at 55 °C. The digested glycogen was acidified with 0.15 N sodium acetate buffer as described above. An aliquot was counted for [^{3}H]-radioactivity, and the remainder was measured for glycogen concentration after amyloglucosidase treatment. The specific activity of glycogen (dpm/μg glycosyl units) was calculated by dividing the [^{3}H]-radioactivity by the glycogen concentration. The amount of 2-DOG incorporation into glycogen was calculated by multiplying the specific activity of glycogen by tissue total glycogen concentration divided by tissue weight. The rate of synthesis from 2-DOG was calculated by dividing the amount of 2-DOG incorporation into glycogen by the AUC of the integrated glucose-specific activity in the plasma during the GTT.

2.6. Pancreas immunofluorescence staining

Pancreas samples were fixed in phosphate-buffered saline (PBS) containing 10% formalin for 24 h, embedded in paraffin, and sectioned (5 μm). The sections were deparaffined and rehydrated (xylene and ethanol) and subjected to antigen retrieval [27] prior to incubation at 4 °C (overnight) with guinea pig anti-insulin (Abcam) or mouse anti-glucagon (Abcam). The sections were then incubated at room temperature with fluorochrome-conjugated secondary antibodies, which were anti-guinea pig Alexa 546 (Invitrogen) or anti-mouse Alexa Fluor 633 (Invitrogen). Images were acquired using a confocal microscope (Zeiss LSM880 Airyscan) and processed with NIH ImageJ.

2.7. Tissue glucose uptake

Tissue-specific glucose uptake was performed using 2-DOG as previously reported [26,28]. 2-DOG has been widely used as a tracer to determine tissue glucose uptake because it is trapped inside the tissues after phosphorylation in the form of [^{3}H]-deoxyglucose-6-phosphate (2-DOG-6-P). As described in Methods 2.5 above, a GTT was performed in 16 h fasted mice with IP injection of 20% dextrose and 2-DOG. The plasma and tissues were harvested, and the integrated glucose-specific activity AUC was calculated. To determine tissue accumulation of 2-DOG-6-P, tissues were weighed and homogenized in 1.2 mL of cold distilled water, and 800 μL of homogenate was transferred to 800 μL ice-cold 1.1 M PCA. The sample was centrifuged to remove precipitated protein, and 1.2 mL of the supernatant was neutralized for 30 min with 300 μL 2.2 M $KHCO_3$. The precipitate was removed by centrifugation, and 1 mL of the supernatant was divided in 500 μL aliquots. One aliquot was used to determine total ^{3}H radioactivity, and the other was passed through an anion exchange column (AG 1-X8 Resin; Bio-Rad) to trap 2-DOG-6-P. The column was washed with distilled water, and the radioactivity in the eluted volume was measured in a scintillation counter. The difference between total and eluted ^{3}H radioactivity represents accumulated [^{3}H]-2-DOG-6-P. To calculate [^{3}H]-2-DOG uptake, the

radioactive counts (degenerations/min) were divided by the integrated glucose-specific activity AUC and the tissue weight.

2.8. Glucose production and signaling in primary hepatocytes

To investigate cell-autonomous mechanisms in the liver, experiments were performed in primary hepatocytes. Male $GNE^{fl/fl}$ mice were injected at 5 weeks of age with AAV8-TBG-GFP or AAV8-TBG-Cre, and 2 weeks later primary hepatocytes were isolated following 16 h fasting according to published protocols [22,29], with minor modifications. In preparation for primary hepatocyte isolation, Perfusion Buffer (calcium and magnesium-free HBSS buffer with 0.5 mM EDTA and 25 mM HEPES) and Digestion Medium (DMEM medium containing 1 g/L glucose, 15 mM HEPES, 1% penicillin/streptomycin and 50 μg/mL collagenase II) were prepared before the perfusion. Mice were anaesthetized by IP injection of ketamine (100 mg/kg), xylazine (10 mg/kg) and acepromazine (2 mg/kg), and a peripheral venous catheter (24 G × 0.75′) was placed in the portal vein. Prior to collagenase infusion, the liver was perfused with Perfusion Buffer at a rate of 3 mL/min via the portal vein after severing the inferior vena cava (IVC). After the color of the liver changed to beige or light brown, Digestion Medium was perfused over 5 min, clamping the IVC for 7–10 s every minute. When the liver surface exhibited cracking and a small indentation occurred with the touch of a cotton swab, the perfusion was stopped and the liver was placed in ice-chilled Digestion Medium. Then the liver was transferred into a biological hood and the gallbladder was carefully removed. The liver sac was ruptured, and the cells were gently released and suspended in Isolation Medium (DMEM medium containing 4.5 g glucose/L, 15 mM HEPES, 2 mM glutamine, 0.1 μM dexamethasone, 1% penicillin/streptomycin and 10% FBS), filtered through a 70 μm cell strainer, and centrifuged at 50 × *g* for 2 min at 4 °C. The cell pellet was washed with Isolation Medium twice and then placed in Percoll (adjusted to physiological ionic strength) at a final concentration of 36%, and centrifuged at 200 × *g* for 10 min. The hepatocyte pellet was washed once with Isolation Medium, and then cultured on collagen I-pre-coated plates in Culture Medium (DMEM containing 1 g/L glucose, 2 mM glutamine, >1 mM sodium pyruvate, 5 mM HEPES, 10 nM dexamethasone, 1% penicillin/streptomycin and 10% FBS) at 37 °C in a humidified CO_2 incubator. After 4 h of attachment the media was changed to warm serum-free Culture Media (without FBS and dexamethasone but with 0.2% BSA). After overnight culture, the hepatocytes were ready for study.

Hepatocyte glucose production was assayed using established methods [30]. Hepatocytes were plated in 12-well plates with 2×10^5 cells per well and cultured overnight in serum free media. Then the cells were washed with Krebs-Ringer-Phosphate-HEPES (KRPH) buffer (20 mM HEPES, 5 mM KH_2PO_4, 1 mM $MgSO_4$, 1 mM $CaCl_2$, 136 mM NaCl, and 4.7 mM KCl, pH 7.4) containing 0.25% BSA to remove glucose and amino acids present in the culture medium. The cells were pre-incubated with 100 nM insulin (Sigma) or 30 nM glucagon (Sigma) or both in a final incubation volume of 500 μL KRPH buffer. After 30 min, gluconeogenic substrates (20 mM lactate, 2 mM pyruvate, 10 mM glutamine) were added to initiate gluconeogenesis and the cells were incubated for an additional 6 h. At the end of the incubation, the culture media was collected for glucose concentration detection using a hexokinase-based glucose assay (ThermoFisher) and for mouse albumin detection by ELISA (abcam). The attached cells were washed three times with cold PBS to remove BSA, dissolved in 1 N KOH and neutralized with 1 N HCl, and protein content per well was determined by BCA assay (ThermoFisher). Alternatively, cells were dissolved in 500 μL of TRIzol reagent (ThermoFisher) for RNA isolation and the subsequent evaluation of gluconeogenesis gene expression. Glucose production was normalized to total protein and expressed as the fold increase from basal glucose output.

To assess signaling in response to insulin, glucagon or forskolin, the cells were treated with 100 nM insulin (Sigma), 30 nM glucagon (Sigma) or 20 μM forskolin (Sigma) in a final incubation volume of 500 μL KRPH buffer. After 15 min, the cells were washed with cold PBS and harvested for homogenization in RIPA buffer supplemented with protease and phosphatase inhibitor cocktail (ThermoFisher). Cell lysates were subjected to immunoblotting or cAMP detection and protein abundance was assessed by BCA assay. To determine the effect of sialic acid supplementation, sialic acid (Sigma) was dissolved in culture medium without serum, the pH was adjusted to neutrality using 1 M NaOH, and the reagent was sterilized using a 0.22 μM filter. Hepatocytes were cultured in medium containing 0.2% BSA and 0.2 nM insulin with or without 5 mM sialic acid added for 3 days. The cells were then washed with KRPH buffer and subjected to insulin or glucagon stimulation as described above.

To assess mechanisms impacting insulin receptor abundance, hepatocytes were treated with the EphB4 inhibitor NVP-BHG712 (Sigma) at 10 nM in medium containing 0.2% BSA and 0.2 nM insulin for 24 h. In additional studies cells were treated with vehicle or the proteasome inhibitor MG132 (10 μM; Sigma), or with vehicle or the lysosome inhibitor NH_4Cl (5 mM) for 18 h. After treatment, insulin signaling was evaluated or the cells were harvested for immunoblotting.

2.9. Glucagon binding assay in primary hepatocytes

The ability of glucagon to bind to the GCGR was evaluated by a competitive binding assay using [^{125}I]-glucagon in mouse primary hepatocytes as previously described [31,32]. In brief, hepatocytes were plated in 24-well plates with 1×10^5 cells per well and cultured overnight in serum-free media including 0.25% BSA. The cells were then washed with KRPH buffer containing 0.25% BSA, and incubated in KRPH buffer with [^{125}I]-glucagon (100 pM, PerkinElmer) and varying concentrations of unlabeled human glucagon (0.001 nM–10 μM, Sigma) at room temperature for 3 h. Cells were washed three times with ice-cold PBS and dissolved by 200 μL of 1 N KOH. After neutralization with 200 μL of 1 N HCl, one aliquot was saved for protein measurement and another was subjected to ^{125}I quantification in a gamma counter. Measurements with 10 μM unlabeled glucagon were used to represent non-specific binding. Specific binding was determined by subtracting non-specific binding and expressed relative to protein content, and disassociation curves were generated.

2.10. Western blotting, lectin blotting and immunoprecipitation

Tissue samples or primary hepatocytes were homogenized in RIPA buffer (ThermoFisher) containing protease and phosphatase inhibitors (ThermoFisher). For western blotting, after SDS-PAGE the proteins were transferred to PVDF membranes and incubated for 1 h in 5% milk blocking buffer. The membranes were then incubated overnight at 4 °C with primary antibodies, followed by incubation with a horseradish peroxidase (HRP)-conjugated secondary antibody. Detected proteins were quantified by densitometry using NIH Image J software.

Lectin blotting was performed to detect sialic acid bound to galactose in α-2,6 or α2,3 linkage, using sambucus nigra lectin (SNA) or maackia amurensis lectin II (MAL-II), respectively, and to detect the β1,4 terminal galactose using erythrina cristagalli lectin (ECL). The procedure mirrored that for western blotting, replacing the western blocking buffer with carbo-free blocking buffer (Vector Lab), incubating the membranes with biotinylated lectins (Vector Lab) overnight, and then detection using an anti-biotin (HRP) second antibody (Vector Lab).

Immunoprecipitation was conducted to evaluate either protein interaction between IR and proteins related to its degradation, or the sialylation of IR or Flag-tagged GCGR in mouse liver. For immunoprecipitation of IR, liver lysates were incubated with control IgG or anti-IRβ antibody (Santa Cruz) at 4 °C overnight. Protein A/G magnetic beads (ThermoFisher) were added, followed by incubation at room temperature for 1 h. The beads conjugated with precipitated proteins were washed three times and collected, and then incubated with Laemmli buffer at room temperature for 15 min to elute the precipitated proteins. In select experiments, before the elution, the beads conjugated with precipitated proteins were treated with 1000 U of α2, 3, 6, 8-neuraminidase (NEB) in 50 μL of 1× GlycoBuffer (NEB) for 24 h at 37 °C to remove the terminal sialic acid. Then western blotting or lectin blotting was performed using the eluted proteins. For immunoprecipitation of flag-tagged GCGR from liver samples, the flag-tagged GCGR was eluted by adding Flag peptide (Sigma) as described previously [33]. The sources of antibodies and reagents are provided in the Supplementary Methods.

2.11. Quantitative RT-PCR (qPCR)

qPCR was performed using established methods [34]. Total RNA was extracted from liver, skeletal muscle, adipose tissue, pancreas or primary hepatocytes using a TRIzol-based method (ThermoFisher). Following reverse transcription, qPCR was carried out using TaqMan Universal Master Mix (ThermoFisher) or SYBR Green Master Mix (ThermoFisher) on a QuantStudio™ 7 Pro Real-Time PCR System (ThermoFisher). Relative mRNA level was calculated by normalizing Ct values to that observed for the housekeeping gene hypoxanthine-guanine phosphoribosyltransferase (HPRT) with the 2ΔΔCt method. The specificity of the PCR amplification was verified by melting curve analysis of the final products using Design and Analysis Software Version 2.6 (ThermoFisher). Primer sequences are provided in the Supplementary Methods.

2.12. Statistical analysis

Statistical analyses were performed using Prism 9 (GraphPad software) or 20.0 (IBM) SPSS (for Two-Way Repeated Measurement ANOVA for four groups). Comparisons between two groups were done by two-tailed unpaired Student's *t*-test for data with normal distribution, and if variance was unequal, Welch's correction was also used. Unpaired Mann—Whitney tests were used to compare two groups for data with non-normal distribution. Comparisons among three or more groups were done with one-way or two-way analysis of variance (ANOVA) with Tukey's post-hoc test for data with normal distribution. Such comparisons were done using Brown-Forsythe and Welch ANOVA tests with Dunnett's T3 multiple comparisons test for data with unequal variance. For comparison between groups with repeated measures, a two-way repeated measures ANOVA was used, followed by Sidak's or Bonferroni multiple comparisons tests. Data are expressed as mean ± SEM, and $P < 0.05$ was considered statistically significant.

3. RESULTS

3.1. Liver GNE deletion increases systemic glucose tolerance

To investigate how sialic acid synthesis in the liver influences glucose homeostasis, we generated floxed GNE mice ($GNE^{fl/fl}$) (Figure S1A and B), and at 5 weeks of age injected them with AAV8 encoding a liver-specific promotor (thyroxine-binding globulin, TBG) driving Cre recombinase to yield mice selectively deficient in liver GNE (GNE^{LKO}). $GNE^{fl/fl}$ injected with AAV8 expressing GFP served as controls (GNE^{WT}). At 2 weeks following virus injection, transcripts for Cre and GFP were exclusively detected in liver (Figure S1C and D), and in GNE^{LKO} mice GNE mRNA and protein levels were decreased 85% and 99% in the liver, respectively, and unchanged in white adipose tissue (WAT), skeletal muscle, and pancreas (Figure S1E—J). Plasma ALT and AST were unaffected by liver GNE deletion (Figure S1K and L), indicating that the loss of GNE does not cause significant hepatocyte injury. As expected, in GNE^{LKO} mice lectin-based analysis using the α2, 6-sialic acid-specific lectin SNA and the α2, 3-sialic acid-specific lectin MAL-II showed reductions in the sialylation of liver and plasma proteins (Figure S2A and B). In parallel, β1,4-galactose-specific lectin ECL blotting showed increased exposure of the terminal galactose on liver and plasma protein glycans. Thus, the sialylation of liver-derived proteins was effectively decreased by hepatic GNE deletion.

Two weeks following virus injection in male chow-fed GNE^{WT} and GNE^{LKO} mice body weights and body composition were comparable (Figure 1A and B). However, in GNE^{LKO} mice fasting glucose was decreased, and glucose tolerance tests (GTT) and insulin tolerance tests (ITT) revealed enhanced glucose and insulin tolerance (Figure 1C—E). The increased glucose tolerance was not related to a change in pancreatic insulin secretion (Figure 1F), and female GNE^{LKO} mice displayed the same changes in fasting glucose, GTT and ITT without alterations in body weight or body composition (Figure S3A—E). A parallel phenotype was also observed in male mice in which liver GNE deficiency was generated by crossing $GNE^{fl/fl}$ mice with mice expressing Cre recombinase under the control of the albumin enhancer/promoter (Alb-Cre) (Figure S3F—J). Furthermore, when the durability of the enhancement in glucose and insulin tolerance with liver GNE deletion was evaluated in male GNE^{LKO} mice, it persisted for at least 12 weeks and food consumption was unaltered over that time period (Figure S3K—R).

Having found that liver GNE deletion increases glucose tolerance in chow-fed lean mice, we determined how the manipulation impacts glucose control in mice with established glucose and insulin intolerance. Following high fat diet (HFD) feeding for 20 weeks, $GNE^{fl/fl}$ mice received either AAV8-TBG-GFP or AAV8-TBG-Cre (Figure 1G). At baseline, the mice assigned to the two study groups had comparable body weight, fasting glucose and GTT (Figure 1H, J, and K). Two weeks following AAV-TBG-Cre injection, without changing body weight or body composition (Figure 1H and I), liver-specific GNE deletion lowered fasting glucose and improved HFD-induced glucose intolerance and insulin resistance (Figure 1J—L). Following hepatic GNE silencing, fasting insulin was also lowered in the HFD-fed mice, and relative pancreatic insulin output in response to a glucose load was unaltered (Figure 1M). Thus, hepatic GNE silencing reversed glucose intolerance and insulin resistance in HFD-fed mice. Collectively these findings indicate that the attenuation of sialic acid production in the liver enhances overall glucose tolerance and insulin sensitivity in the setting of either standard diet feeding or established HFD-induced insulin resistance.

3.2. Liver GNE deletion blunts hepatic insulin sensitivity by increasing IR degradation

To further evaluate tissue-specific insulin sensitivity, hyperinsulinemic—euglycemic clamp studies were performed in chow-fed GNE^{WT} and GNE^{LKO} male mice. The amount of exogenous glucose required to maintain euglycemia (glucose infusion rate, GIR) was similar in the two groups (Figure 2A), and insulin suppression of hepatic glucose production (HGP), which reflects hepatic insulin sensitivity, was impaired in GNE^{LKO} mice (Figure 2B and C). Having found decreased hepatic insulin sensitivity, we evaluated possible alterations in insulin signaling. The phosphorylation of insulin receptor β (IRβ),

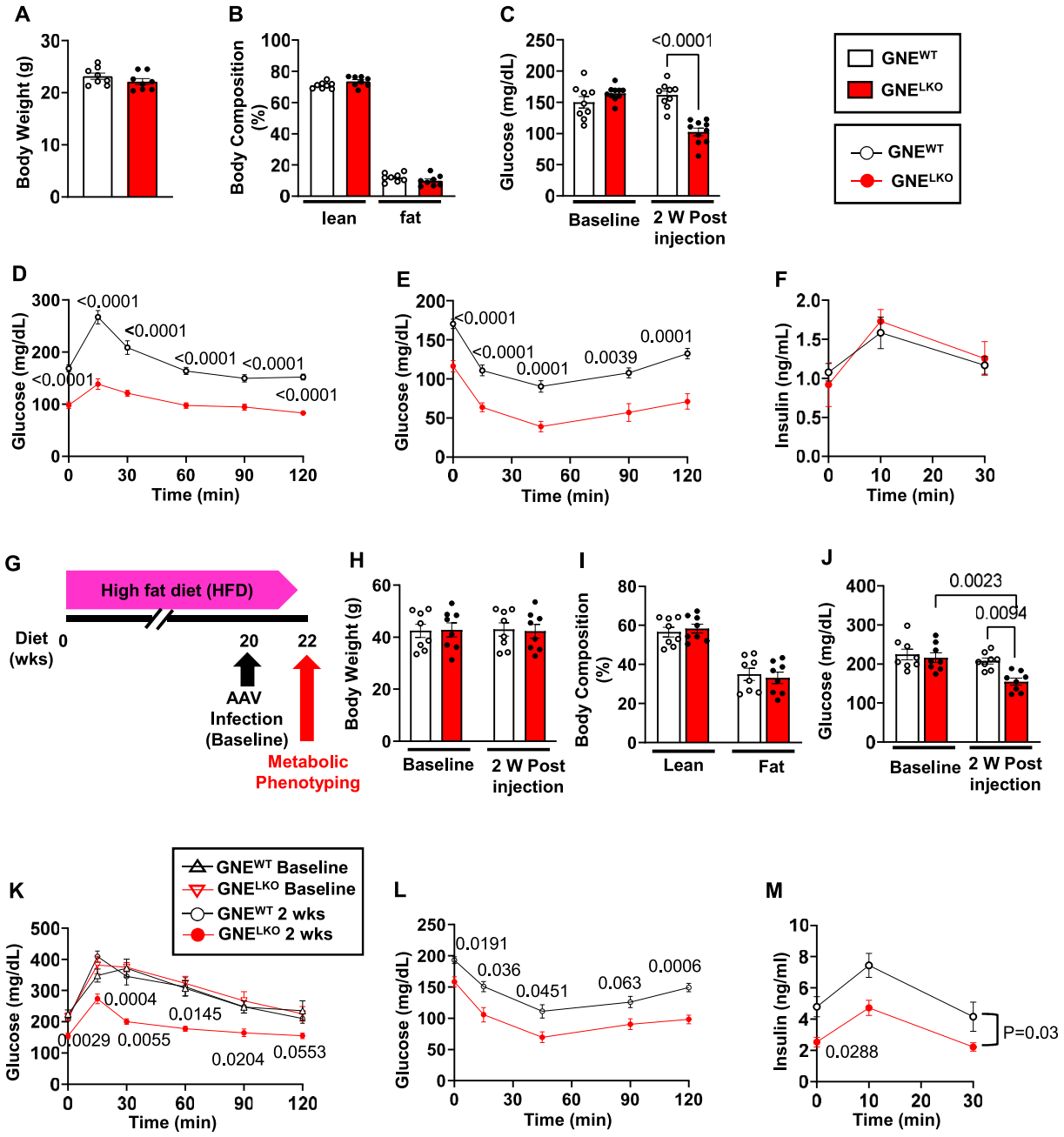

Figure 1: Hepatocyte-specific deletion of GNE improves glucose tolerance and insulin sensitivity. A, B. Male GNE$^{fl/fl}$ mice were injected with control AAV8-GFP or AAV8-Cre at 5 weeks of age, and fed control diet for 2 weeks. Body weights (A, N = 8/group), and lean and fat mass (B, N = 8/group). C. Plasma glucose concentrations after 6 h fast measured at baseline and 2 weeks post AAV8 injection (N = 9,10/group). D. Glucose tolerance tests (1 g/kg glucose) after 6 h fast, 2 weeks post AAV8 injections (N = 15,16/group). E. Insulin tolerance tests (0.5 U/kg insulin) after 6 h fast, 2 weeks post AAV8 injections (N = 15/group). F. Insulin secretion during GTT was measured in mice after 6 h fast (N = 8/group). G–M. After 20 weeks on HFD, male GNE$^{fl/fl}$ mice were injected with control AAV8-GFP or AAV8-Cre, and fed HFD for additional 2 weeks (G). Body weights measured at baseline and 2 weeks post AAV8 injection (H, N = 8/group) and body composition (I) measured 2 weeks post AAV8 injection (N = 8/group). J. Plasma glucose concentration after 6 fast measured at baseline and 2 weeks post AAV8 injection. (N = 8/group). K. Glucose tolerance tests (1 g/kg glucose) after 6 h fast at baseline and 2 weeks post AAV8 injections. (N = 8/group). L. Insulin tolerance tests (0.5 U/kg insulin) after 6 h fast, 2 weeks post AAV8 injections (N = 8/group). M. Insulin secretion during GTT measured in mice after 6 h fast (N = 8/group). Data are represented as mean ± SEM. Significance was determined by unpaired two-tailed Student's t test (A, B, I), two-way ANOVA with Tukey's multiple comparison test (C, H, J), two-way repeated measures ANOVA with Sidak's multiple-comparison analysis (D–F, K–M). In D, E and L the p values are shown for comparisons at individual time points between the two study groups. In K, p values are shown for comparisons at a given time point between the two study groups tested at 2 weeks post-AAV8 injection. In M, p values are shown for the comparison between the two study groups at baseline (0 min), and for the findings over the entire 30 min.

Akt, and GSK-3α/β in the liver at the end of the clamp was decreased in GNE^{LKO} mice (Figure 2D and E). The attenuated signaling downstream of the insulin receptor was related to a decrease in the abundance of insulin receptor subunits α and β (IRα and IRβ), which occurred in the absence of a change in the abundance of the precursor of insulin receptor (Pro-IR) or in IR mRNA expression (Figure 2D–F).

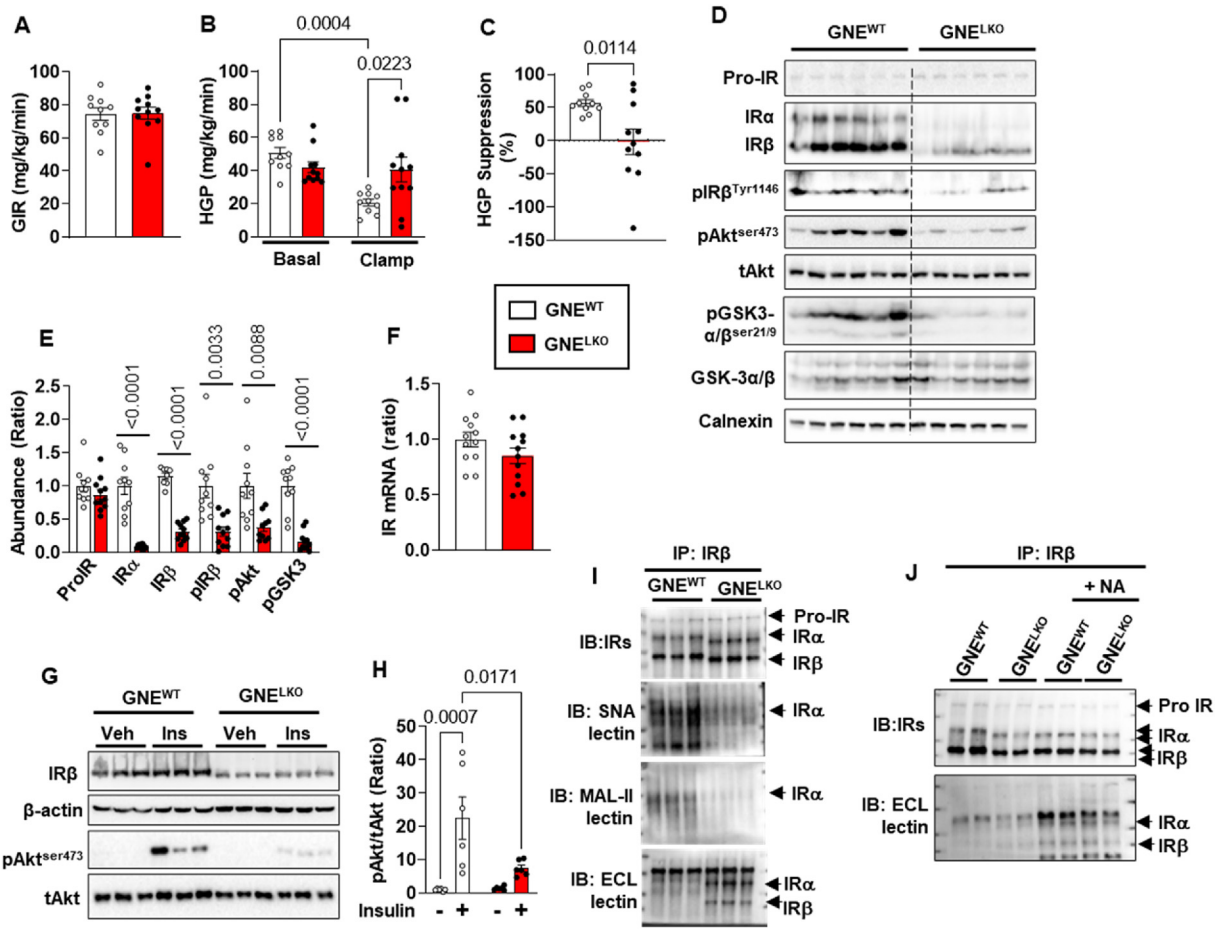

Figure 2: Hepatocyte-specific deletion of GNE decreases insulin receptor (IR) sialylation and protein levels, and impairs IR signaling in the liver. A—C. Male GNE$^{fl/fl}$ mice were injected with control AAV8-GFP or AAV8-Cre at 5 weeks of age, and fed control diet for 2—4 weeks. Hyperinsulinemic—euglycemic clamps were performed, and glucose infusion rate (GIR, A), hepatic glucose production (HGP, B) and HGP suppression rates (C) were measured (N = 10,11/group). D, E. After the clamp, livers were isolated, and expression of IR precursor (Pro-IR), IRα and IRβ, phosphorylation of IRβ-Tyr1146, Akt-Ser473 and GSK3α/β-Ser21/9 were assessed by immunoblot (D). E. Quantitation by densitometry (N = 8—11/group). F. Insulin receptor (IR) mRNA expression in the liver by qRT-PCR (N = 12/group). G—H. Two weeks post AAV8 injection, mice were injected with vehicle (PBS) or insulin (2 U/kg, 5 min), and liver Akt-ser473 phosphorylation and insulin receptor expression were assessed by immunoblot (G). H. Quantitation by densitometry for phosphorylated Akt (N = 6/group). I. Insulin Receptors (IR) were immunoprecipitated from liver lysate, and IR sialylation and galactosylation were assessed by SNA-lectin, MAL-II lectin or ECL-lectin blotting. Findings for 3 samples per group are shown. J. Separate sets of immunoprecipitated IRβ were treated with neuraminidase (NA), and its electromobility and terminal galactosylation were assessed by IRα/IRβ immunoblot and ECL-lectin blot. Findings for 2 samples per group are shown. Data are represented as mean ± SEM. Significance was determined by unpaired two tailed Student's t test (A, Pro-IR and IRβ in E, F), unpaired two tailed Student's t test with Welch's correction (C, IRα, pIRβ, pAkt and pGSK3 in E) and two-way ANOVA with Tukey's multiple comparison analysis (B, H).

Likewise, in studies of acute in vivo responses to insulin, accompanying the loss of IR in the livers of GNE^{LKO} mice, Akt phosphorylation in response to insulin was attenuated (Figure 2G and H).

Both IRα and IRβ are glycosylated, and cell culture studies indicate that modifications in the glycans play a critical role in maintaining insulin receptor abundance and subcellular localization [11,35—38]. To assess the contribution of GNE and sialylation to IR glycan structure in vivo, IRβ was immunoprecipitated and gel electrophoresis and lectin blotting were performed. In the livers of GNE^{LKO} mice, both IRα and IRβ displayed increased mobility in the gel electrophoresis, α2,6-linked sialylation and α2,3-linked sialylation were both decreased, and in parallel there was greater detection of terminal galactose (Figure 2I). After removal of the terminal sialic acid by neuraminidase treatment of immunoprecipitated IR, GNE^{LKO} IR and GNE^{WT} IR subunits migrated at an identical molecular mass and terminal galactose detection was comparably increased (Figure 2J). This indicates that the observed differences in IR protein size with GNE deficiency relate to altered sialylation.

To evaluate whether the demonstrated alterations in IR function are hepatocyte-autonomous, we studied primary hepatocytes isolated from GNE^{WT} and GNE^{LKO} mice. Protein hyposialyation was observed in the hepatocytes from GNE^{LKO} mice (Figure S2C), IRα and IRβ molecular weight and abundance were decreased (Figure S4A and B), and insulin-stimulated phosphorylation of IRβ, Akt and GSK-3 was blunted (Figure S4C—F). The treatment of GNE^{LKO} hepatocytes with sialic acid normalized not only the molecular weight and abundance of IRα and IRβ, but also insulin activation of IRβ phosphorylation (Figure S4G—J). These collective findings indicate that in GNE^{LKO} liver, hyposialylation of IRα and IRβ results in a decrease in the abundance of the proteins, leading to the attenuation of insulin action in hepatocytes.

We further determined how hyposialylation causes the decrease in insulin receptor abundance in hepatocytes. Since the abundance of

Pro-IR was not changed by GNE silencing in the liver (Figure 2D and E, Figure S4A and B), indicating that the maturation of IR was not impacted by hyposialylation, the degradation of the receptor was evaluated. IRβ was immunoprecipitated from liver lysates from GNE^{WT} and GNE^{LKO} mice, and the ubiquitination of IRα and IRβ was evaluated. The loss of GNE did not alter IRα or IRβ ubiquitination (Figure S4K). The possible role of altered proteasomal degradation was also interrogated in primary hepatocytes. Treatment with the proteasome inhibitor MG132 did not change the abundance of IRα or IRβ in GNE^{LKO} hepatocytes (Figure S4L–N). Thus, the loss of hepatic IRα and IRβ in the setting of hyposialylation is not due to changes in proteasomal degradation of the receptor subunits. A second mode of insulin receptor degradation involves the tyrosine kinase receptor Eph receptor B4 (EphB4). In hepatocytes, insulin causes an increase in EphB4 direct interaction with the insulin receptor to recruit it to the adaptor protein 2 (Ap2) complex to promote clathrin-mediated endocytosis and degradation of the receptor in lysosomes [39]. Although GNE^{LKO} and GNE^{WT} livers have equal abundance of EphB4, clathrin and the Mu 1 subunit of the Ap2 complex (Ap2M1), the immunoprecipitation of IRβ from GNE^{LKO} liver yielded 2-fold or greater coimmunoprecipitation of EphB4, clathrin and Ap2M1 (Figure 3A–C). In addition, the treatment of GNE^{LKO} hepatocytes with the small molecule inhibitor of EphB4, NVP-BHG712 (NVP), caused the recovery of IRα and IRβ abundance to the levels normally found in GNE^{WT} hepatocytes, without affecting their molecular weights (Figure 3D–F). In parallel, the inhibition of lysosomal degradation with NH_4Cl also rescued normal abundance of IRα and IRβ (Figure 3G–I). Therefore, with GNE deletion there is a decrease in hepatic insulin sensitivity, and it is due to hyposialylation of the insulin receptor, which leads to its enhanced degradation by EphB4 and a resulting decline in insulin signaling.

3.3. Liver GNE deletion attenuates hepatic GCGR action by decreasing affinity for glucagon

Having found that changes in hepatic insulin sensitivity do not explain the enhancement of global glucose tolerance observed with liver GNE silencing, we evaluated possible alterations in glucagon action. Changes in glucagon receptor function in particular were sought when it was determined that in GNE^{LKO} mice serum glucagon levels are increased by 11-, 18-, and 9-fold after feeding, 6-hours fasting or 16-hours fasting, respectively (Figure 4A and Figure S5A). The plasma level of GLP-1, a hormone produced by proglucagon through prohormone convertases [40,41] was also increased 2-fold in GNE^{LKO} mice (Figure S5B). Pancreas weight, immunofluorescence for glucagon-producing α cells, and glucagon gene (*Gcg*) expression were additionally markedly increased in GNE^{LKO} mice (Figure S5C–F). Since these findings mirror the phenotype of GCGR knockout mice [42–44], we determined if liver GCGR function is altered in GNE^{LKO} mice by performing glucagon tolerance tests (GcTT). Whereas blood glucose rose rapidly in response to exogenous glucagon in GNE^{WT} mice, GNE^{LKO} mice failed to exhibit a response (Figure 4B). Responses to GcTT were also absent in female GNE^{LKO} mice and in male $GNE^{fl/fl}$;Albumin Cre mice (Figure S5G and H). Thus, GNE deletion causes an attenuation of glucagon action in the liver, and there is a compensatory increase in pancreatic glucagon production.

To determine the basis for the loss of glucagon action with liver GNE silencing, GCGR signaling was studied. In non-fasting GNE^{LKO} mice glucagon failed to elicit increases in hepatic cAMP, PKA activation and PKA substrate phosphorylation (Figure 4C–F), and there was a compensatory upregulation in GCGR transcript abundance (Figure 4G). In parallel, in primary hepatocytes from GNE^{LKO} mice glucagon stimulation of cAMP production and PKA substrate phosphorylation was attenuated (Figure 4H–J), indicating that the effect of GNE deficiency on glucagon signaling in hepatocytes is cell-autonomous. Knowing that GCGR are G protein-coupled to adenylyl cyclase [45], the process in receptor action altered by GNE deficiency was evaluated by interrogating the direct response of adenyl cyclase to forskolin [45,46]. cAMP production and PKA substrate phosphorylation in response to forskolin were identical in GNE^{LKO} and GNE^{WT} hepatocytes (Figure 4K–M). Strengthening the evidence that hyposialylation is the basis for the impairment in glucagon action in the setting of GNE silencing, treatment with sialic acid normalized glucagon-induced cAMP production and PKA substrate phosphorylation in GNE^{LKO} primary hepatocytes (Figure 5A–C). These findings indicate that the loss of GNE adversely impacts GCGR function and not processes distal to the receptor.

To determine the basis for hepatic GCGR dysfunction, using AAV8, a flag- and myc-tagged GCGR was expressed in vivo in the livers of GNE^{WT} or GNE^{LKO} mice. A decrease in GCGR molecular weight was observed in GNE^{LKO} liver without affecting the abundance of the tagged receptor (Figure 5D and E). Using the flag-tag to isolate the GCGR, SNA, MAL-II and ECL lectin blotting all revealed a marked reduction in GCGR sialylation in GNE^{LKO} liver (Figure 5F). To then interrogate the basis for GCGR dysfunction related to hyposialylation, competitive binding assays were performed on primary hepatocytes from GNE^{WT} and GNE^{LKO} mice after the hepatocytes were treated with either vehicle or sialic acid (Figure 5G). Bmax revealed that GCGR density is similar in GNE^{WT} and GNE^{LKO} hepatocytes, and also not affected by the provision of exogenous sialic acid (Figure 5H). However, Kd was 10-fold greater in GNE^{LKO} versus GNE^{WT} hepatocytes in the absence of sialic acid, and it was normalized in GNE^{LKO} hepatocytes by the provision of exogenous sialic acid (Figure 5I). These collective observations reveal that GNE deletion in the liver causes hyposialylation of the GCGR, which does not alter receptor abundance but instead decreasing the affinity of the GCGR for glucagon, leading to the attenuation of glucagon action.

3.4. Liver GNE deletion alters liver glucose production and storage

Having found that both insulin and glucagon action in the liver are decreased by GNE silencing, the cumulative impact of GNE deletion on hepatic glucose production and storage was interrogated. To evaluate gluconeogenesis, pyruvate tolerance tests (PTT) were performed, and they revealed that gluconeogenesis from pyruvate is reduced in GNE^{LKO} mice after 16 h fasting (Figure 6A). In parallel, the key enzymes in gluconeogenesis, glucose-6-phosphatase (G6pc) and phosphoenolpyruvate carboxykinase (PEPCK, Pck1) were downregulated in the livers of fasting GNE^{LKO} mice compared to fasting GNE^{WT} mice (Figure 6B and C). These findings may be related to the loss of glucagon action in GNE^{LKO} liver. Interestingly, the suppression of G6pc and Pck1 expression in response to refeeding was also attenuated with liver GNE silencing (Figure 6B and C), possibly reflecting the decreased responses to insulin observed in the GNE^{LKO} liver. Plasma non-esterified fatty acid (NEFA) levels were similar in GNE^{WT} and GNE^{LKO} mice under both fasting and fed conditions (Figure 6D), indicating that changes in gluconeogenesis are not due to alterations in NEFA modulation of the process.

To evaluate glucose storage, liver glycogen content was measured, and it was decreased in GNE^{LKO} mice after GTT and under both fasting and fed conditions (Figure 6E and F). To evaluate if this is related to lower glycogenesis, ^{3}H-2-deoxy-glucose (2DOG) incorporation into glycogen and glycogen synthesis rate were determined (Figure 6G and H), and they were both lower in GNE^{LKO} mice. In addition, the upregulation of glucokinase with feeding was attenuated with liver GNE silencing, resulting in decreased glucose-6-phosphate for glycogenesis (Figure 4I). These findings related to glycogenesis likely reflect the marked decrease in hepatic insulin signaling observed in the GNE^{LKO} mice.

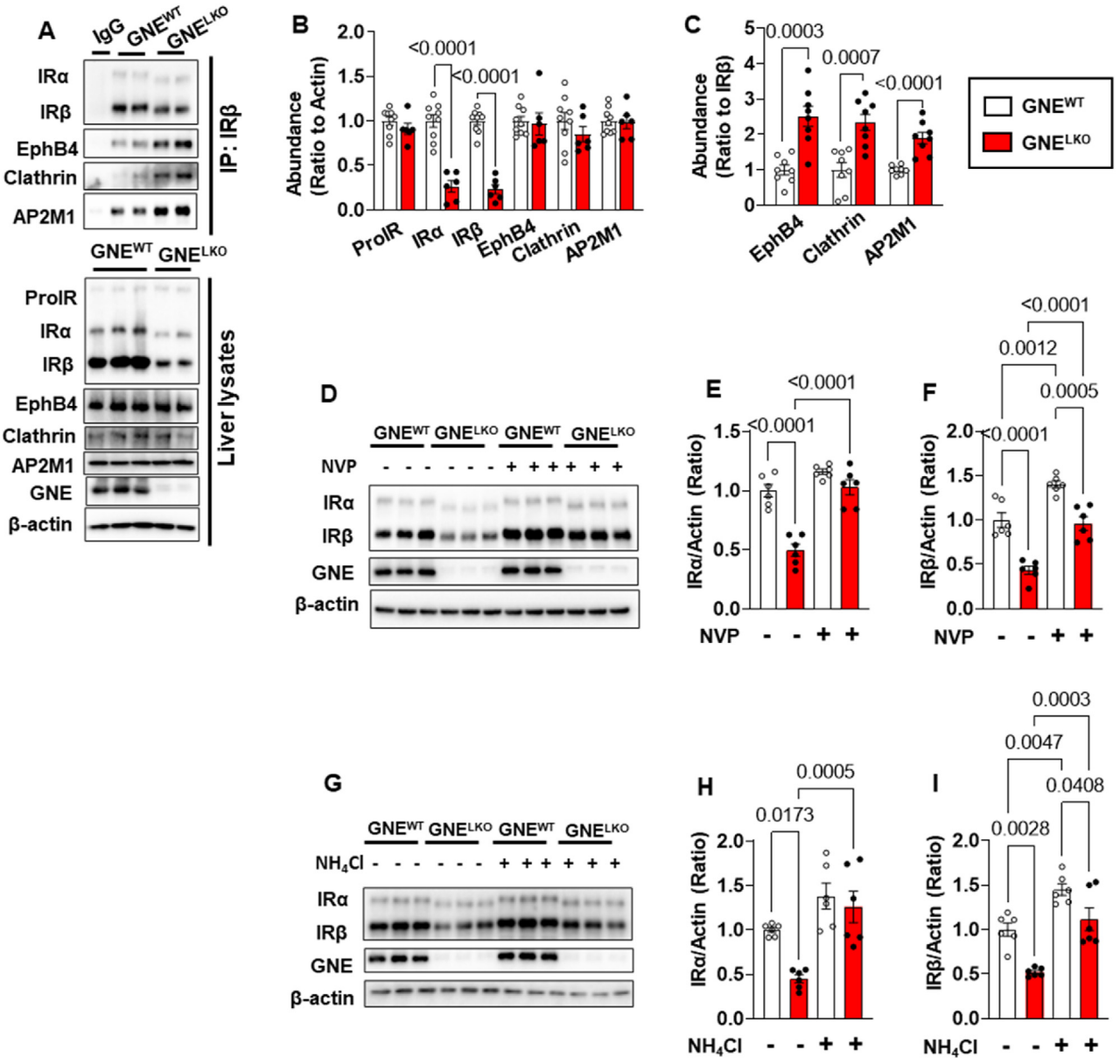

Figure 3: Hepatocyte-specific deletion of GNE promotes the IR degradation in the liver. A–C. Male GNE$^{fl/fl}$ mice were injected with control AAV8-GFP or AAV8-Cre at 5 weeks of age, and fed control diet for 2 weeks. Mice were fasted for 16 h followed by 4 h refeed, the livers were isolated and the abundance of IRs, EphB4, Clathrin and AP2M1 were assessed by immunoblot after IR immunoprecipitation or in whole liver lysates (A). Quantitation by densitometry in the whole liver lysates (B, N = 6–9/group) or after IR immunoprecipitation (C, N = 8/group). D–I. Male GNE$^{fl/fl}$ mice were injected with control AAV8-GFP or AAV8-Cre at 5 weeks of age, and fed control diet for 2 weeks, and primary hepatocytes were isolated. The cells were treated with/without 10 nM EphB4 inhibitor NVP (D–F) for 24 h, or with/without 5 mM lysosome inhibitor NH_4Cl for 18 h (G–I). The expression of IRα and IRβ were assessed by immunoblot (N = 6/group). Quantitation of immunoblots by densitometry is shown in E, F, H, and I. Data are represented as mean ± SEM. Significance was determined by unpaired two tailed Student's t test (B and Clathrin in C), unpaired two tailed Student's t test with Welch's correction (EphB4 and Ap2M1 in C) and one-way ANOVA with Tukey's multiple comparison analysis (E–F, H–I).

To evaluate if the changes in glucose production and storage with hepatocyte GNE loss are cell-autonomous, the release of glucose from isolated hepatocytes was interrogated. In wild-type cells glucose release and G6pc and Pck1 expression were all upregulated by glucagon, and the responses to glucagon were attenuated by concurrent cell treatment with insulin (Figure 6J–L). In contrast, the effects of glucagon and insulin were lost in hepatocytes from GNE^{LKO} mice. Albumin secretion was unaffected by GNE-deficiency (Figure 6M), indicating that the overall function of the hepatocytes was unaltered. The combination of in vivo and ex vivo observations indicate that the inhibition of sialic acid synthesis in the liver alters both glucose production and storage in hepatocytes.

Considering that insulin and glucagon regulate hepatic lipid metabolism [47,48], an impact of liver GNE deletion on plasma and liver lipids was investigated. In the ad libitum fed state plasma levels of triglyceride (TG) were decreased by 41% in GNE^{LKO} mice, and plasma levels of NEFA and total cholesterol (TC), and hepatic TG, TC and NEFA abundance were unchanged (Figure 6D and Figure S6A–E). In the

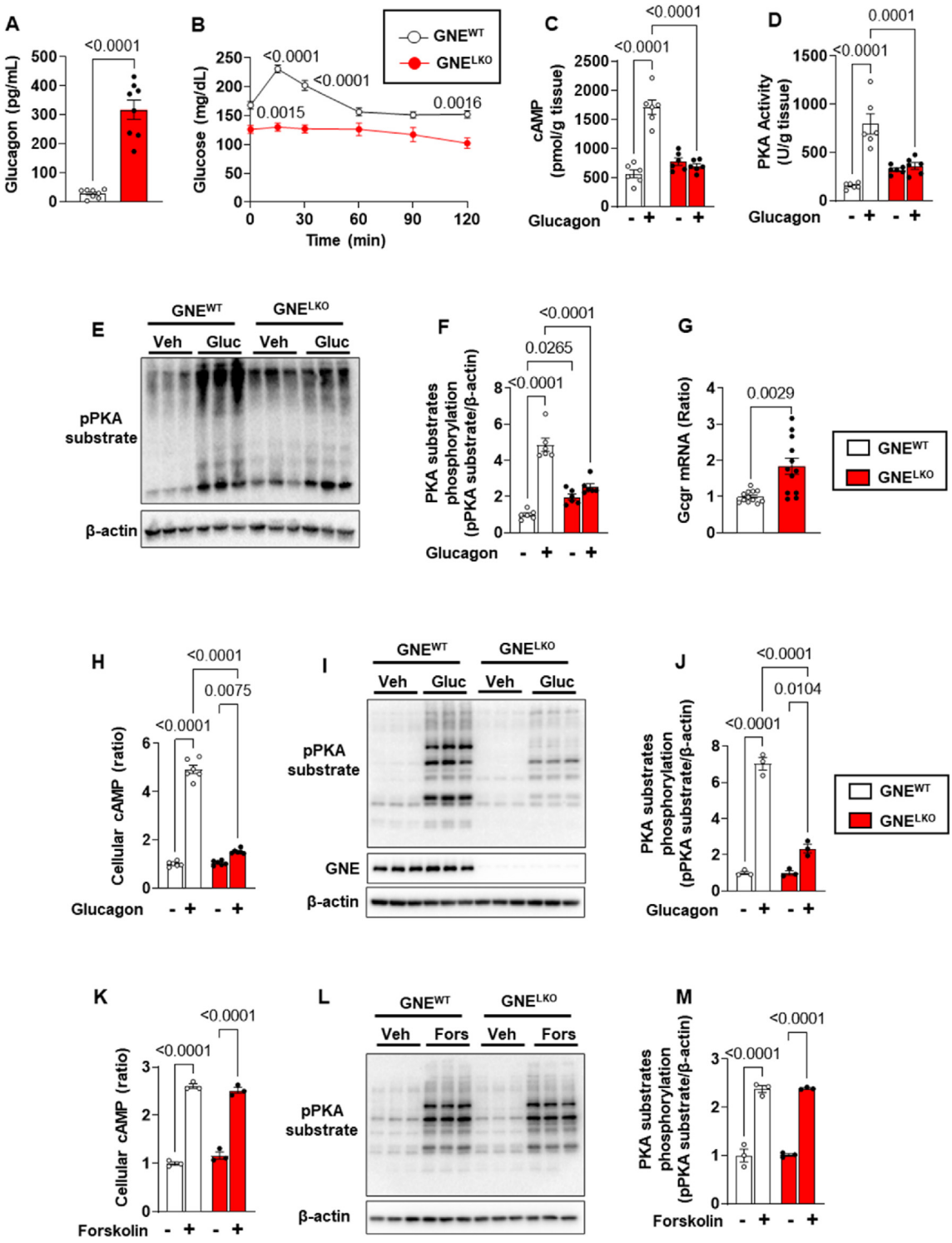

Figure 4: Hepatocyte-specific deletion of GNE attenuates glucagon receptor (GCGR) signaling in the liver. A. Male GNE$^{fl/fl}$ mice were injected with control AAV8-GFP or AAV8-Cre at 5 weeks of age, and fed control diet for 2 weeks. Plasma glucagon levels in fed mice (N = 8/group). B. Glucagon tolerance tests (16 μg/kg glucagon) were performed in mice after 6 h fast (N = 12/group). C–F. GCGR downstream signaling pathway. After injections of vehicle (PBS) or glucagon (1 mg/kg), cAMP levels (C), PKA activity (D) and phosphorylation of PKA substrates (E, F) in the liver were evaluated (N = 6/group). G. GCGR mRNA expression in the liver by qRT-PCR (N = 12/group). H–J. Male GNE$^{fl/fl}$ mice were injected with control AAV8-GFP or AAV8-Cre at 5 weeks of age and fed control diet for 2 weeks. Primary hepatocytes were isolated and cultured for 24 h, and treated with glucagon (30 nM) for 15 min. Cellular cAMP levels were measured (H, N = 6/group) and phosphorylation of PKA substrates was also assessed by immunoblot (I, 3 samples per group are shown). Quantitation of immunoblots is shown in J (N = 3/group). K–M. Primary hepatocytes were treated with vehicle or 20 μM forskolin for 15 min, the cellular cAMP production was measured (K, N = 3/group) and the phosphorylation of PKA substrates were assessed by immunoblot (L). Quantitation of immunoblots by densitometry is shown in M (N = 3/group). Data are represented as mean ± SEM. Significance was determined by unpaired two-tailed Student's t test with Welch's correction (A, G), or two-way ANOVA with Tukey's multiple comparison test (C, D, F, H, J–K and M), or by two-way repeated measures ANOVA with Sidak's multiple comparison test (B).

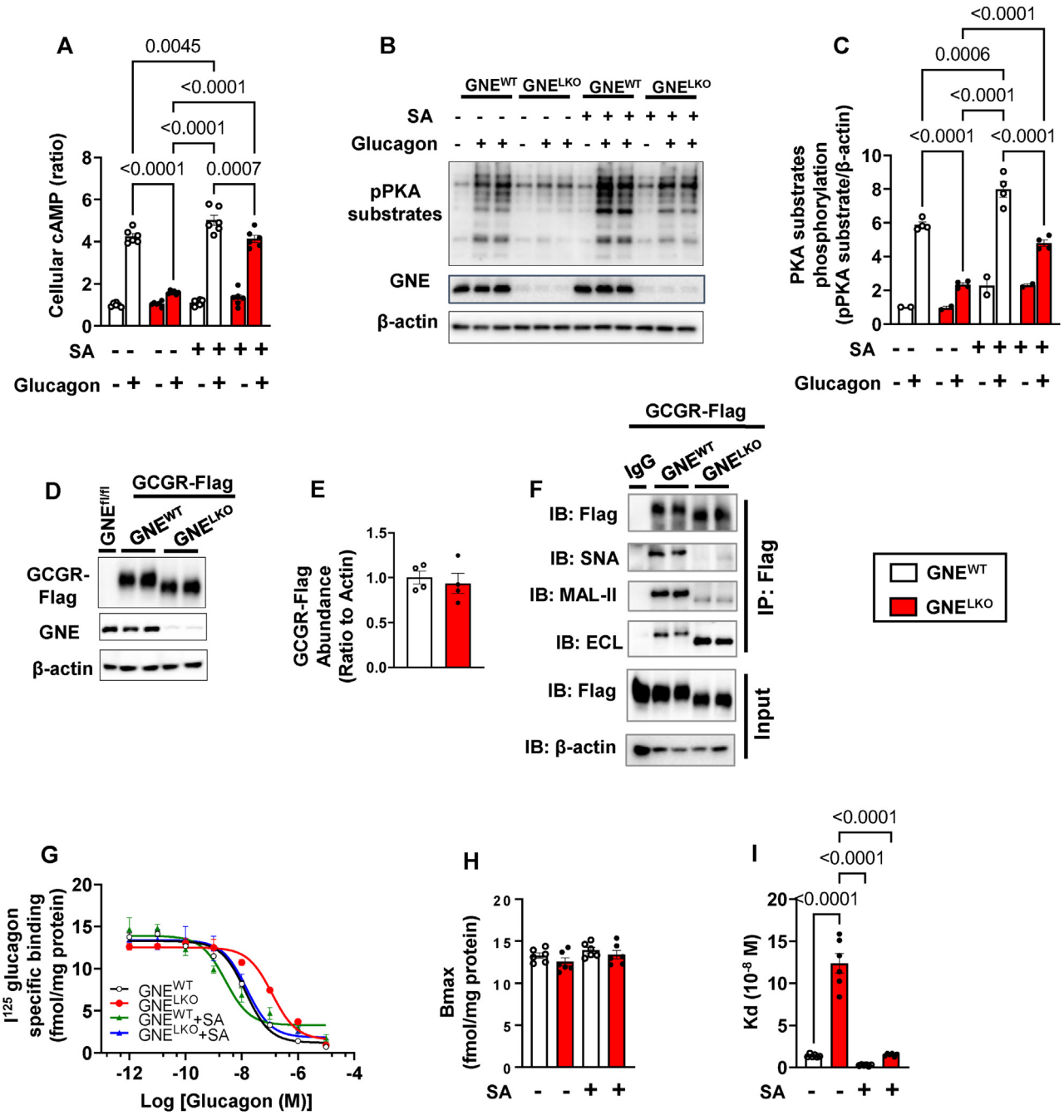

Figure 5: Hepatocyte-specific deletion of GNE attenuates glucagon receptor sialylation and it affinity to glucagon. A–C. Male GNE$^{fl/fl}$ mice were injected with control AAV8-GFP or AAV8-Cre at 5 weeks of age and fed control diet for 2 weeks. Primary hepatocytes were isolated and cultured for 24 h, and pretreated with/without 5 mM sialic acid for 3 days followed by 15 min of glucagon (30 nM) treatment, and the cellular cAMP levels (A, N = 6/group) were measured and phosphorylation of PKA substrates was assessed by immunoblot (B). Quantitation of immunoblots is shown in C (N = 2 or 4/group). D–F. Male GNE$^{fl/fl}$ mice were injected with AAV8 expressing Flag- and Myc-tagged GCGR followed by administration of control AAV8-GFP or AAV8-Cre at 5 weeks of age, and fed control diet for 2 weeks. Expression of Flag-tagged GCGR was determined by immunoblot (D, E, N = 4/group). Flag-tagged GCGR was immunoprecipitated from liver lysates using anti-Flag antibody, and the receptor sialylation and galactosylation were assessed by SNA-lectin, MAL-II lectin or ECL-lectin blotting. Two samples per group are shown in F. G–I. In another set of experiments hepatocytes were pretreated with/without 5 mM sialic acid for 3 days, then [^{125}I]-Glucagon binding assay was performed (N = 6/group). The binding curve, maximal binding sites and dissociation constant Kd were shown in G–I. Data are represented as mean ± SEM. Significance was determined by unpaired two-tailed Student's t test with Welch's correction (E), or one-way ANOVA (H, I) or two-way ANOVA with Tukey's multiple comparison test (A, C).

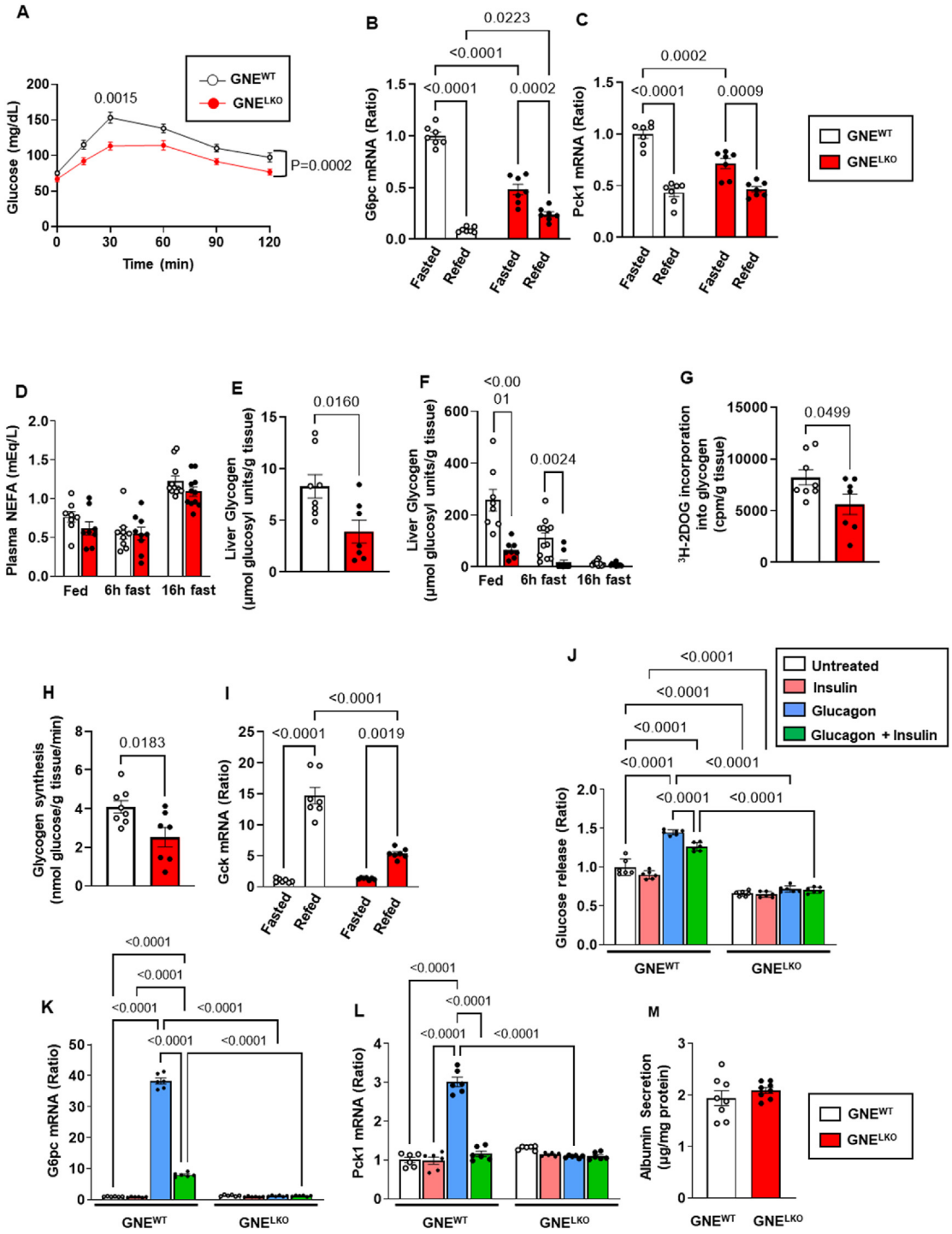

Figure 6: Liver GNE deletion alters liver glucose production and storage. A. Male GNE$^{fl/fl}$ mice were injected with control AAV8-GFP or AAV8-Cre at 5 weeks of age, and fed control diet for 2 weeks. Pyruvate tolerance tests (2 g/kg, body weight) were performed after 16 h fast (N = 13, 14/group). B, C. Expression of G6pc (B) or Pck1 (C) mRNA by qRT-PCR in the liver of mice after 16 h fast (Fasted) or after 16 h fast followed by 4 h refeed (Refed). N = 7/group. D. Plasma NEFA levels in fed mice or mice after 6 h or 16 h fast (N = 8–11). E. Following GTT in mice after 16 h fast, glycogen levels in the liver were measured (N = 8,7/group). F. Liver glycogen levels in fed mice or mice after 6 h or 16 h fast (N = 8–12/group). G, H. Following GTT in mice after 16 h fast, [^{3}H]-2-deoxyglucose incorporation into glycogen (G) and glycogen synthesis rate (H) were measured (N = 8,7/group). I. Expression of Gck mRNA by qRT-PCR in the liver of mice after 16 h fast (Fasted) or after 16 h fast followed by 4 h refeed (Refed) (N = 7/group). J. Mouse primary hepatocytes were treated with vehicle, insulin (100 nM), glucagon (30 nM) or both for 30 min, followed by additional 6 h incubation in the presence of the substrates (20 mM lactate, 2 mM pyruvate, 10 mM glutamine). Glucose in culture buffer was measured (N = 6/group). K, L. Mouse primary hepatocytes were treated with vehicle, insulin (100 nM), glucagon (30 nM) or both for 6 h, and expression of G6pc (K) and Pck1 (L) was evaluated by qRT-PCR (N = 6/group). M. Albumin secretion was measured 24 h post isolation (N = 8). Data are represented as mean ± SEM. Significance was determined by two-way repeated measures ANOVA with Sidak's multiple comparison test (A), two-way ANOVA with Tukey's multiple comparison test (B, C, D, F, I–L), unpaired two-tailed Student's t test (E, G, H), or unpaired two-tailed Student's t test with Welch's correction (M). In A, p values are shown for the comparison between the two study groups at the single 30 min time point, and for the findings over the entire 120 min.

fasted state, plasma TG levels were similar between GNE^{WT} and GNE^{LKO} mice, and after acute refeeding TG levels were reduced 55% in GNE^{LKO} compared to GNE^{WT} mice (Figure S6F). Plasma NEFA and TC and hepatic TG, TC and NEFA levels were not altered by liver GNE deletion during fasting or refeeding (Figure S6G—K). Thus, the primary observation for liver lipid metabolism was that the inhibition of sialic acid synthesis decreases plasma TG levels in the fed state.

3.5. Liver GNE deletion promotes peripheral insulin sensitivity by increasing FGF21 production

Along with revealing alterations in glucose homeostasis in the liver in GNE^{LKO} mice, the hyperinsulinemic-euglycemic clamps indicated that both the glucose disposal rate (GDR) and the insulin-stimulated glucose disposal rate (IS-GDR), which primarily reflects skeletal muscle insulin sensitivity, were increased in the GNE^{LKO} mice (Figure 7A and B). In addition, 2-DOG uptake during a GTT was increased in extensor digitorum longus (EDL) and soleus muscle in GNE^{LKO} mice (Figure 7C), and at the end of the clamp the phosphorylation of IRβ, Akt, and GSK-3α/β in soleus was increased (Figure 7D and E). In contrast, in white adipose tissue (WAT) at the end of the clamp insulin suppression of lipolysis and IRβ, Akt, and GSK-3α/β phosphorylation were similar in GNE^{WT} mice and GNE^{LKO} mice (Figure S7A—D). Therefore, insulin sensitivity was unchanged in WAT and increased in skeletal muscle in GNE^{LKO} mice.

Seeking an explanation for how alterations in sialic acid biosynthesis in the liver impact skeletal muscle insulin sensitivity, plasma levels of fibroblast growth factor 21 (FGF21) were measured, and under both fasting and fed conditions FGF21 was markedly elevated in GNE^{LKO} mice (Figure 7F). This was related to a 3.3-fold increase in FGF21 mRNA selectively in the liver (Figure 7G). There was an accompanying 39% decrease in the forkhead box protein O1 (FoxO1) protein abundance and a loss of insulin-induced phosphorylation of FoxO1 (Figure S8A—C), possibly explaining why FGF21 was upregulated [49—51]. Expression of the FGF21 receptor (FGFR1) and co-receptor β-Klotho (KLB) were unaltered in various target tissues of FGF21 action (Figure S9A and B). To determine if the upregulation of hepatic FGF21 production underlies the increase in muscle insulin sensitivity in GNE^{LKO} mice, liver FGF21 was silenced concurrently with liver GNE. Compared to control mice (GNE^{WT}) and mice deficient only in liver GNE (GNE^{LKO}), plasma FGF21 levels were predictably minimal in mice lacking only liver FGF21 ($FGF21^{LKO}$) or both hepatic GNE and FGF21 (GNE^{LKO};$FGF21^{LKO}$) (Figure 7H). Without changes in body weight, body composition or food consumption (Figure S9C—E), blood glucose was normalized by 63% and there was reversal of the enhanced skeletal muscle glucose uptake and insulin signaling in GNE^{LKO} mice with concurrent liver FGF21 silencing (Figure 7I—L). Whereas GcTT were not normalized in GNE^{LKO};$FGF21^{LKO}$ mice (Figure 7M), changes in GTT and ITT with liver GNE deletion were negated with simultaneous loss of liver FGF21 (Figure 7N and O). Thus, in addition to decreasing hepatic insulin sensitivity and glucagon action, liver GNE deletion promotes skeletal muscle insulin sensitivity and glucose disposal by increasing hepatic FGF21 production. Recognizing that the composite effect of liver GNE silencing is a global increase in glucose tolerance and insulin sensitivity, these findings have revealed multiple mechanisms in the liver by which sialic acid influences glucose control.

4. DISCUSSION

Although glycosylation is a major mode of post-translational modification of proteins [52] and lipids [4], little is known about how the process influences systemic metabolic processes. There are possible mechanistic links between sialic acid production and protein sialylation in the liver and glucose homeostasis because the glycans on key hepatic proteins governing glucose metabolism, including the insulin receptor (IR) and glucagon receptor (GCGR), are terminally sialylated [11—13]. However, it has been entirely unknown whether sialic acid production and the process of sialylation in the liver influence glucose homeostasis. To fill that knowledge gap we deleted UDP-N-acetylglucosamine-2-epimerase/N-acetylmannosamine kinase (GNE), the rate-limiting enzyme in sialic acid production from glucose, selectively from the liver in mice. The resulting decrease in hepatic sialic acid production and sialylation caused an attenuation of insulin action in the liver related to a decline in IRα and IRβ abundance, leading to lower glycogenesis. The decrease in GNE activity and sialic acid production also caused a blunting of hepatic GCGR function, yielding declines in both gluconeogenesis and glycogenolysis (Figure 8). As a result of upregulation of FGF21 expression, hepatic GNE deletion also caused an enhancement of skeletal muscle glucose disposal which led to an overall positive impact on glucose tolerance and insulin sensitivity. The increased overall glucose control occurred with liver GNE silencing in both lean mice and mice with established insulin resistance caused by diet-induced obesity. Thus, sialic acid synthesis and sialylation in the liver modulate multiple facets of glucose homeostasis.

The loss of hepatic IR abundance and action with liver GNE knockdown was related to a decrease in its sialylation. The IR is heavily glycosylated with multiple species of complex of N-linked glycans which are required for proper folding, maturation, targeting and activity of the receptor [11,35—38]. Whereas a prior study of purified IRα and IRβ showed that their desialylation with neuraminidase causes an increase in insulin binding and kinase activity [53], neuraminidase treatment of primary rat hepatocytes caused a decrease in insulin-stimulated lipogenesis [54]. In vivo in mice, whereas global genetic deficiency of neuraminidase 1 (NEU1) causes a decrease in insulin sensitivity, the pharmacologic activation of NEU1 results in either decreased or increased insulin sensitivity depending on the duration of treatment [13,55]. Compared to those works, the present study has the advantages that through the manipulation of organ-specific GNE expression, sialic acid synthesis and the degree of sialylation have been modified with temporal control specifically in the liver in vivo. Although it is not possible to manipulate the sialylation of IR exclusively, IR hyposialylation and deficiency and their consequences were demonstrated in parallel. In primary hepatocytes from GNE^{LKO} livers normal IR abundance and signaling were recovered by sialic acid treatment, strengthening the link between sialylation and receptor availability and function. We further determined that the decline in IRα and IRβ abundance caused by hyposialylation is due to enhanced recruitment of the IR to Eph receptor B4, leading to increased targeting of the receptor for lysosomal degradation.

In addition to revealing how sialic acid synthesis influences IR abundance and function in the liver, the present work provides new insights into how sialic acid impacts the actions of glucagon in hepatocytes. The GCGR is glycosylated, and available data in mice has shown that Mgat5, a Golgi N-acetylglucosaminyltransferase that modulates N-glycan branching, alters GCGR glycan structure resulting in the attenuation of glucagon binding and downstream signaling [12]. How sialylation per se impacts GCGR and its function has been unknown. We demonstrate that a loss of hepatocyte sialic acid synthesis results in hyposialylation of the GCGR and a blunting of hepatic glucagon action that is related to a decrease in receptor affinity for glucagon. In evaluations of hepatic cAMP, PKA and PKA substrate responses, we determine that the loss of liver sialic acid production impairs GCGR stimulation of adenylate cyclase. However, responses to forskolin are not altered with hepatocyte GNE knockdown, further implicating

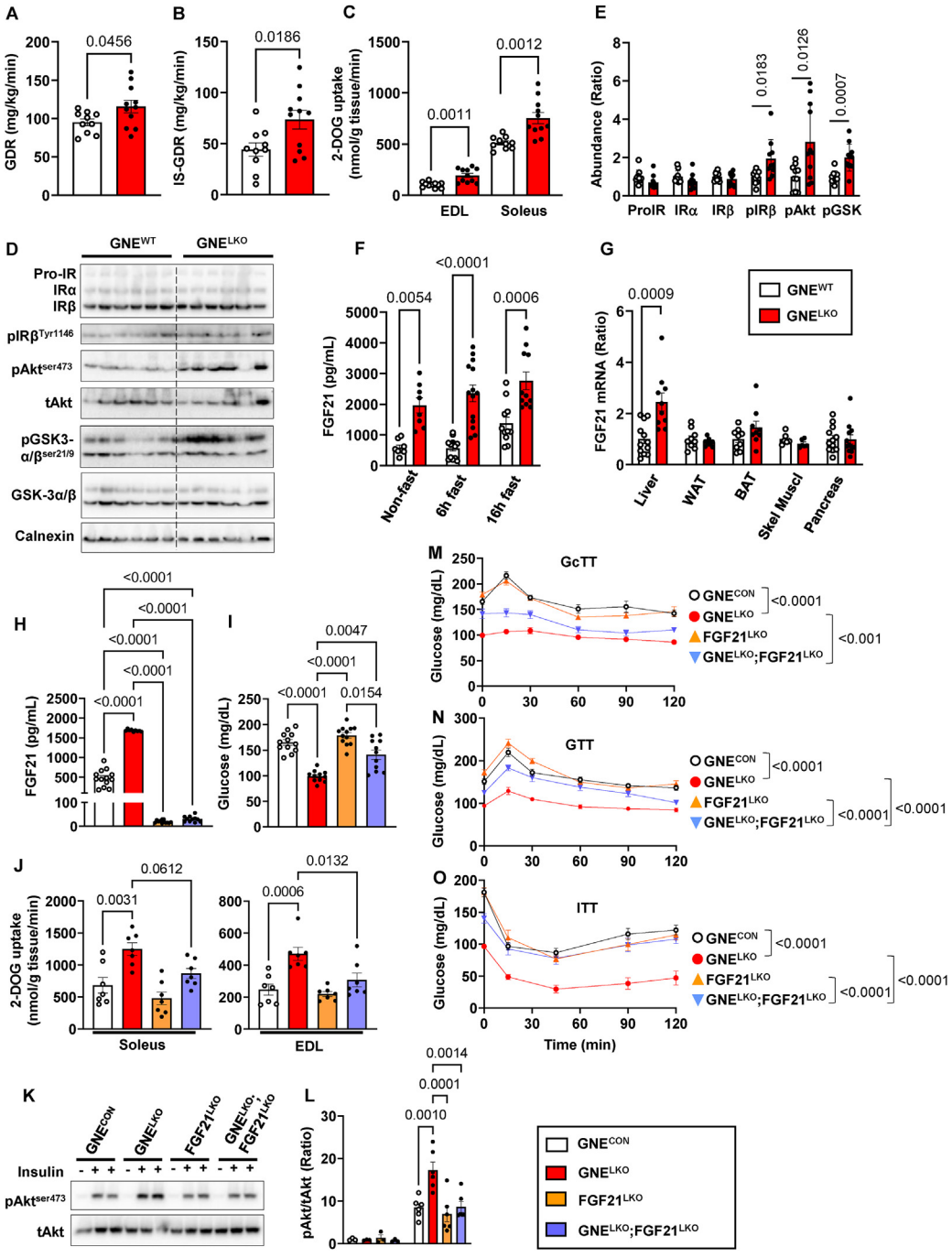

Figure 7: Hepatocyte-specific deletion of GNE promotes insulin signaling and glucose uptake in the skeletal muscle by causing increased hepatic production of FGF21. A, B. Male GNE$^{fl/fl}$ mice were injected with control AAV8-GFP or AAV8-Cre at 5 weeks of age, and fed control diet for 2–4 weeks. Glucose disposal rate (GDR, A) and insulin-stimulated glucose disposal rate (IS-GDR, B) during hyperinsulinemic–euglycemic clamp (N = 10–11/group). C. During a GTT [^{3}H]-2-deoxyglucose uptake was evaluated in the extensor digitorum longus (EDL) and soleus muscles (N = 10–11/group). D, E. Insulin receptor (IR) expression and signaling downstream of IR were evaluated following the clamp by immunoblot (E). Quantitation of immunoblots is shown in E (N = 10–11/group). F, G. Plasma FGF21 concentrations in mice without fasting or after 6 h or 16 h fast (F, N = 8–14/group). FGF21 mRNA expression levels were evaluated by qRT-PCR in liver, white adipose tissue (WAT), brown adipose tissue (BAT), skeletal muscle (Skel Muscl) and pancreas (G, N = 6–12/group). H, I. Male GNE$^{fl/fl}$, FGF21$^{fl/fl}$ or GNE$^{fl/fl}$;FGF21$^{fl/fl}$ mice were injected with control AAV8-GFP or AAV8-Cre at 5 weeks of age, and fed control diet for 2 week. Plasma FGF21 levels (H, N = 9–13/group) and plasma glucose levels after 6 h fast (I, N = 11–12/group). J. During a GTT [^{3}H]-2-deoxyglucose uptake was evaluated in soleus and EDL skeletal muscle (N = 7/group). K, L. Two weeks post AAV8 injection, mice were injected with vehicle (PBS) or insulin (0.5 U/kg, 5 min), and Akt-ser473 phosphorylation in the soleus were assessed by immunoblot (K). Quantitation by densitometry for phosphorylated Akt (L, N = 3–6/group). M. Glucagon tolerance tests (16 μg/kg glucagon) after 6 h fast at 2 weeks post AAV8 injections (N = 11–12/group). N. Glucose tolerance tests (1 g/kg glucose) after 6 h fast at 2 weeks post AAV8 injection (N = 11–12/group). O. Insulin tolerance tests (0.5 U/kg insulin) after 6 h fast at 2 weeks post AAV8 injection (N = 11–12/group). Data are represented as mean ± SEM. Significance was determined by unpaired two tailed Student's t test (A, B, ProIR, IRα and IRβ in E, G), unpaired two tailed Student's t test with Welch's correction (C, pIRβ, pAkt, pGSK in E), one-way ANOVA with Tukey's multiple comparison (J), Brown-Forsythe and Welch ANOVA with Dunnett's T3 multiple comparisons test (H, I), two-way ANOVA with Tukey's multiple comparison test (F, L), or two-way repeated measures ANOVA with Bonferroni multiple comparison test to compare blood glucose among groups (M–O).

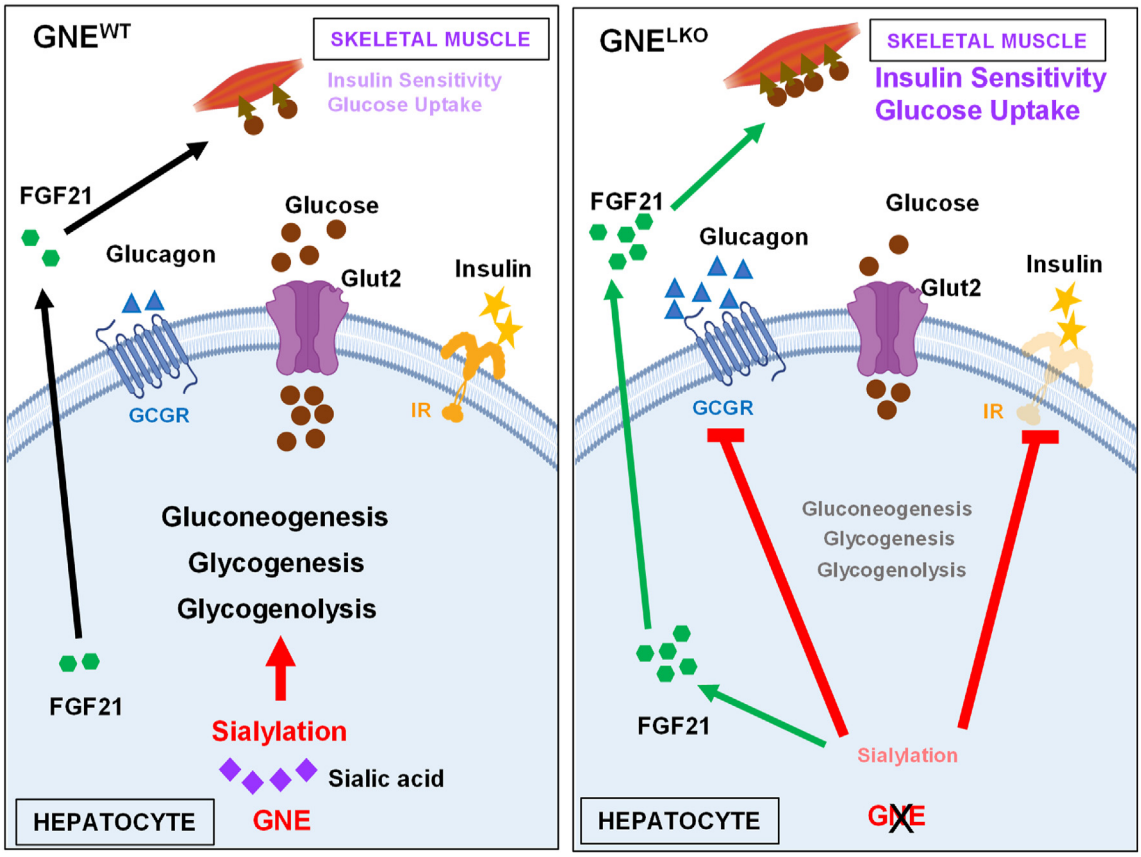

Figure 8: Impact of hepatic sialic acid synthesis by GNE and sialylation on liver glucose metabolism and peripheral insulin sensitivity. With GNE silencing in hepatocytes the resulting decrease in hepatic sialic acid production and sialylation causes an attenuation of insulin action in the liver related to a decline in IRα and IRβ abundance, leading to lower glycogenesis. The decrease in GNE activity and sialic acid production also causes a blunting of hepatic GCGR function, yielding declines in both gluconeogenesis and glycogenolysis. As a result of upregulation of hepatic FGF21 expression, there is an enhancement of skeletal muscle glucose uptake which leads to an overall positive impact on glucose tolerance and insulin sensitivity. Thus, sialic acid synthesis and sialylation in the liver modulate multiple facets of glucose homeostasis. The figure was generated using BioRender.com.

alterations at the level of GCGR. Prompted by the dramatic, 10-fold change in affinity observed with GNE silencing and the importance of liver glucagon action to overall glucose control, further studies are now warranted to determine how GCGR affinity for glucagon is influenced by sialic acid and sialylation. An additional observation was that decreasing liver sialic acid production causes a decrease in plasma TG in the fed state. Although this may be due to the observed decrease in insulin signaling in the liver, because insulin promotes de novo lipid synthesis in the postprandial state [47,56], its basis is still to be determined.

Along with influencing glucose homeostasis within the liver, we discovered that hepatic sialic acid production has potent impact on peripheral insulin sensitivity, and this was related to the modulation of skeletal muscle glucose disposal. We determined that liver GNE silencing causes a substantial upregulation of hepatic FGF21 production, and concurrent manipulation of hepatic GNE and FGF21 showed that the increased FGF21 production is the basis for the enhanced muscle glucose delivery and overall increases in glucose tolerance and insulin sensitivity with decreased hepatic sialic acid production (Figure 8). The upregulation in FGF21 expression with GNE silencing may have been due to an accompanying decrease in FoxO1 expression [49–51]. Why FoxO1 is downregulated with a decrease in liver sialic acid production will need to be pursued in future studies. The increase in skeletal muscle glucose uptake dependent on increased FGF21 in GNE^{LKO} mice is consistent with previous studies indicating that FGF21 promotes peripheral glucose disposal both in adipose tissues and skeletal muscle [50,57,58]. There was an associated FGF21-dependent promotion of insulin signaling in muscle, suggesting that the FGF21 effect was insulin-related. However, interpreting the changes in muscle Akt activation as indicative of altered insulin action may not be straightforward, because it is uncertain whether Akt signaling is required for insulin effects in muscle [59–61], and muscle insulin sensitivity can vary without changes in Akt phosphorylation [62]. An alternative explanation for FGF21 effect on muscle is that it is indirect, occurring through effects on adipose tissues [58,63].

Overall, the present finding that the genetic manipulation of hepatic sialic acid production in mice perturbs glucose homeostasis may have relevance to glucose control in humans. Numerous clinical studies have demonstrated an inverse relationship between plasma protein sialylation and glucose tolerance and insulin sensitivity [64–72], mirroring the directionality that we observed in mice. Since most circulating proteins are liver derived, their relative sialylation may reflect the degree of sialic acid influence on hepatic mechanisms of glucose control. Now with greater mechanistic understanding in hand, one possibility worthy of consideration is that alterations in plasma protein sialylation in humans can serve as a biomarker reflecting the presence or future risk of insulin resistance because they are an

indicator of changes in liver sialic acid synthesis that influence glucose homeostasis.

The current findings also have potential therapeutic relevance because the favorable impact of inhibiting hepatic sialic acid synthesis and protein sialylation on overall glucose control is substantial, and demonstrable even when enacted long after the development of insulin resistance due to diet-induced adiposity. Although the hepatic insulin resistance that occurs after liver GNE knockdown is not therapeutically favorable, it is greatly outweighed by the inhibition of glucagon action and the enhancement of peripheral insulin sensitivity. Inhibition of glucagon receptor signaling has been investigated as a glucose-lowering strategy for type 2 diabetes [73]. However, potential adverse effects of GCGR blockade on hepatic lipid accumulation and elevations of liver aminotransferases have hampered the approach as a type 2 diabetes therapy [48,73,74]. Interestingly, in GNE^{LKO} mice, the loss of GCGR function in liver did not induce hepatic steatosis or increase circulating aminotransferases. On the contrary, a loss of liver GNE lowers plasma TG without affecting hepatic TG levels. These findings suggest that the inhibition of hepatic GNE activity may be a potential therapeutic modality to improve glucose homeostasis and insulin sensitivity without adversely affecting lipid metabolism. In addition, now knowing that hepatic GNE activity robustly influences glucagon action and muscle glucose disposal, the more detailed underpinnings can be investigated to reveal more specific new means to target actions of sialic acid including protein sialylation in the liver to improve glycemic control.

5. CONCLUSIONS

The present work reveals that there is a metabolic cycle comprised of glucose conversion to sialic acid and sialic acid influence on glucose homeostasis. Further interrogation of this cycle, both systemically and in specific cell types such as hepatocytes, will continue to provide valuable information about unknown aspects of glucose homeostasis and the critical role that glycobiology plays in metabolism.

AUTHOR CONTRIBUTIONS

Conceptualization: JP, DO, JJK, WLH, PWS, CM, *Methodology*: JP, LY, CM, *Validation*: JP, LY, HC, LH, *Formal Analysis*: JP, XX, LX, CM, *Investigation*: JP, LY, VP, CS, HC, LH, WLH, *Resources*: DO, JJK, LX, *Writing (Original and revised drafts)*: JP, PWS, CM, *Writing (Review & Editing)*: DO, JJK, LX, WLH, *Visualization:* JP, PWS, CM, *Supervision*: PWS, CM, *Project Administration*: PWS, CM, *Funding Acquisition*: DO, JJK, LX, WLH, PWS, CM.

DECLARATION OF COMPETING INTEREST

The authors declare that they have no known competing financial interests or personal relationships that could have appeared to influence the work reported in this paper.

DATA AVAILABILITY

Data will be made available on request.

ACKNOWLEDGMENTS

This work was supported by National Institutes of Health grants R01-DK110127 (CM) and R01-HL115122 (PWS), R01-DK108773 (DYO), R01-DK112826 (WLH), R21-CA259771 and HG-011996 (LX), R35-GM145599 (JJK), P30DK127984 (UTSW Mouse Metabolic Phenotyping Core), American Heart Association Postdoctoral Fellowship 19POST34390001 (JP), the Rally Foundation (LX), Children's Cancer Fund (LX), Cancer Prevention and Research Institute of Texas (CPRIT) grants RP180319, RP200103, RP220032, RP170152, and RP180805 (LX).

APPENDIX A. SUPPLEMENTARY DATA

Supplementary data to this article can be found online at https://doi.org/10.1016/j.molmet.2023.101812.

REFERENCES

[1] Varki A. Sialic acids in human health and disease. Trends Mol Med 2008;14(8):351–60.
[2] Traving C, Schauer R. Structure, function and metabolism of sialic acids. Cell Mol Life Sci 1998;54(12):1330–49.
[3] Varki A, Gagneux P. Multifarious roles of sialic acids in immunity. Ann N Y Acad Sci 2012;1253:16–36.
[4] Schnaar RL, Sandhoff R, Tiemeyer M, Kinoshita T. Glycosphingolipids. In: Varki A, Cummings RD, Esko JD, Stanley P, Hart GW, Aebi M, et al., editors. Essentials of glycobiology. 4th ed. Cold Spring Harbor (NY); 2022. p. 129–40.
[5] Hinderlich S, Stasche R, Zeitler R, Reutter W. A bifunctional enzyme catalyzes the first two steps in N-acetylneuraminic acid biosynthesis of rat liver. Purification and characterization of UDP-N-acetylglucosamine 2-epimerase/N-acetylmannosamine kinase. J Biol Chem 1997;272(39):24313–8.
[6] Stasche R, Hinderlich S, Weise C, Effertz K, Lucka L, Moormann P, et al. A bifunctional enzyme catalyzes the first two steps in N-acetylneuraminic acid biosynthesis of rat liver. Molecular cloning and functional expression of UDP-N-acetyl-glucosamine 2-epimerase/N-acetylmannosamine kinase. J Biol Chem 1997;272(39):24319–24.
[7] Pham ND, Pang PC, Krishnamurthy S, Wands AM, Grassi P, Dell A, et al. Effects of altered sialic acid biosynthesis on N-linked glycan branching and cell surface interactions. J Biol Chem 2017;292(23):9637–51.
[8] Schwarzkopf M, Knobeloch KP, Rohde E, Hinderlich S, Wiechens N, Lucka L, et al. Sialylation is essential for early development in mice. Proc Natl Acad Sci U S A 2002;99(8):5267–70.
[9] Rudman N, Gornik O, Lauc G. Altered N-glycosylation profiles as potential biomarkers and drug targets in diabetes. FEBS Lett 2019;593(13):1598–615.
[10] Dotz V, Wuhrer M. N-glycome signatures in human plasma: associations with physiology and major diseases. FEBS Lett 2019;593(21):2966–76.
[11] Klaver E, Zhao P, May M, Flanagan-Steet H, Freeze HH, Gilmore R, et al. Selective inhibition of N-linked glycosylation impairs receptor tyrosine kinase processing. Dis Model Mech 2019;12(6).
[12] Johswich A, Longuet C, Pawling J, Abdel Rahman A, Ryczko M, Drucker DJ, et al. N-glycan remodeling on glucagon receptor is an effector of nutrient sensing by the hexosamine biosynthesis pathway. J Biol Chem 2014;289(23):15927–41.
[13] Dridi L, Seyrantepe V, Fougerat A, Pan X, Bonneil E, Thibault P, et al. Positive regulation of insulin signaling by neuraminidase 1. Diabetes 2013;62(7):2338–46.
[14] Samuel VT, Shulman GI. The pathogenesis of insulin resistance: integrating signaling pathways and substrate flux. J Clin Invest 2016;126(1):12–22.
[15] Ramnanan CJ, Edgerton DS, Kraft G, Cherrington AD. Physiologic action of glucagon on liver glucose metabolism. Diabetes Obes Metab 2011;13(Suppl 1):118–25.
[16] Geng L, Lam KSL, Xu A. The therapeutic potential of FGF21 in metabolic diseases: from bench to clinic. Nat Rev Endocrinol 2020;16(11):654–67.
[17] Kehlenbrink S, Koppaka S, Martin M, Relwani R, Cui MH, Hwang JH, et al. Elevated NEFA levels impair glucose effectiveness by increasing net hepatic glycogenolysis. Diabetologia 2012;55(11):3021–8.

[18] Carrillo N, Malicdan MC, Huizing M. GNE myopathy: etiology, diagnosis, and therapeutic challenges. Neurotherapeutics 2018;15(4):900–14.
[19] Ran FA, Hsu PD, Wright J, Agarwala V, Scott DA, Zhang F. Genome engineering using the CRISPR-Cas9 system. Nat Protoc 2013;8(11):2281–308.
[20] Titchenell PM, Chu Q, Monks BR, Birnbaum MJ. Hepatic insulin signalling is dispensable for suppression of glucose output by insulin in vivo. Nat Commun 2015;6:7078.
[21] Byun S, Seok S, Kim YC, Zhang Y, Yau P, Iwamori N, et al. Fasting-induced FGF21 signaling activates hepatic autophagy and lipid degradation via JMJD3 histone demethylase. Nat Commun 2020;11(1):807.
[22] Li P, Liu S, Lu M, Bandyopadhyay G, Oh D, Imamura T, et al. Hematopoietic-derived galectin-3 causes cellular and systemic insulin resistance. Cell 2016;167(4):973–984.e912.
[23] Paschoal VA, Walenta E, Talukdar S, Pessentheiner AR, Osborn O, Hah N, et al. Positive reinforcing mechanisms between GPR120 and PPARγ modulate insulin sensitivity. Cell Metab 2020;31(6):1173–1188.e1175.
[24] Virkamäki A, Rissanen E, Hämäläinen S, Utriainen T, Yki-Järvinen H. Incorporation of [3-3H]glucose and 2-[1-14C]deoxyglucose into glycogen in heart and skeletal muscle in vivo: implications for the quantitation of tissue glucose uptake. Diabetes 1997;46(7):1106–10.
[25] Mauvais-Jarvis F, Virkamaki A, Michael MD, Winnay JN, Zisman A, Kulkarni RN, et al. A model to explore the interaction between muscle insulin resistance and beta-cell dysfunction in the development of type 2 diabetes. Diabetes 2000;49(12):2126–34.
[26] Zisman A, Peroni OD, Abel ED, Michael MD, Mauvais-Jarvis F, Lowell BB, et al. Targeted disruption of the glucose transporter 4 selectively in muscle causes insulin resistance and glucose intolerance. Nat Med 2000;6(8):924–8.
[27] Ying W, Lee YS, Dong Y, Seidman JS, Yang M, Isaac R, et al. Expansion of islet-resident macrophages leads to inflammation affecting beta cell proliferation and function in obesity. Cell Metab 2019;29(2):457–474 e455.
[28] Tanigaki K, Sacharidou A, Peng J, Chambliss KL, Yuhanna IS, Ghosh D, et al. Hyposialylated IgG activates endothelial IgG receptor FcγRIIB to promote obesity-induced insulin resistance. J Clin Invest 2018;128(1):309–22.
[29] Charni-Natan M, Goldstein I. Protocol for primary mouse hepatocyte isolation. STAR Protoc 2020;1(2):100086.
[30] Miller RA, Chu Q, Xie J, Foretz M, Viollet B, Birnbaum MJ. Biguanides suppress hepatic glucagon signalling by decreasing production of cyclic AMP. Nature 2013;494(7436):256–60.
[31] Siu FY, He M, de Graaf C, Han GW, Yang D, Zhang Z, et al. Structure of the human glucagon class B G-protein-coupled receptor. Nature 2013;499(7459):444–9.
[32] Weston C, Lu J, Li N, Barkan K, Richards GO, Roberts DJ, et al. Modulation of glucagon receptor Pharmacology by receptor activity-modifying protein-2 (RAMP2). J Biol Chem 2015;290(38):23009–22.
[33] Valdez-Sinon AN, Gokhale A, Faundez V, Bassell GJ. Protocol for immunoenrichment of FLAG-tagged protein complexes. STAR Protoc 2020;1(2):100083.
[34] Huang L, Chambliss KL, Gao X, Yuhanna IS, Behling-Kelly E, Bergaya S, et al. SR-B1 drives endothelial cell LDL transcytosis via DOCK4 to promote atherosclerosis. Nature 2019;569(7757):565–9.
[35] Elleman TC, Frenkel MJ, Hoyne PA, McKern NM, Cosgrove L, Hewish DR, et al. Mutational analysis of the N-linked glycosylation sites of the human insulin receptor. Biochem J 2000;347(Pt 3):771–9.
[36] Hwang JB, Hernandez J, Leduc R, Frost SC. Alternative glycosylation of the insulin receptor prevents oligomerization and acquisition of insulin-dependent tyrosine kinase activity. Biochim Biophys Acta 2000;1499(1–2):74–84.
[37] Sparrow LG, Gorman JJ, Strike PM, Robinson CP, McKern NM, Epa VC, et al. The location and characterisation of the O-linked glycans of the human insulin receptor. Proteins 2007;66(2):261–5.
[38] Sparrow LG, Lawrence MC, Gorman JJ, Strike PM, Robinson CP, McKern NM, et al. N-linked glycans of the human insulin receptor and their distribution over the crystal structure. Proteins 2008;71(1):426–39.
[39] Liu X, Wang K, Hou S, Jiang Q, Ma C, Zhao Q, et al. Insulin induces insulin receptor degradation in the liver through EphB4. Nat Metab 2022;4(9):1202–13.
[40] Janah L, Kjeldsen S, Galsgaard KD, Winther-Sørensen M, Stojanovska E, Pedersen J, et al. Glucagon receptor signaling and glucagon resistance. Int J Mol Sci 2019;20(13).
[41] Holst JJ, Bersani M, Johnsen AH, Kofod H, Hartmann B, Orskov C. Proglucagon processing in porcine and human pancreas. J Biol Chem 1994;269(29):18827–33.
[42] Gelling RW, Du XQ, Dichmann DS, Romer J, Huang H, Cui L, et al. Lower blood glucose, hyperglucagonemia, and pancreatic alpha cell hyperplasia in glucagon receptor knockout mice. Proc Natl Acad Sci U S A 2003;100(3):1438–43.
[43] Lee Y, Wang MY, Du XQ, Charron MJ, Unger RH. Glucagon receptor knockout prevents insulin-deficient type 1 diabetes in mice. Diabetes 2011;60(2):391–7.
[44] Okamoto H, Cavino K, Na E, Krumm E, Kim SY, Cheng X, et al. Glucagon receptor inhibition normalizes blood glucose in severe insulin-resistant mice. Proc Natl Acad Sci U S A 2017;114(10):2753–8.
[45] Habegger KM, Heppner KM, Geary N, Bartness TJ, DiMarchi R, Tschop MH. The metabolic actions of glucagon revisited. Nat Rev Endocrinol 2010;6(12):689–97.
[46] Seamon KB, Padgett W, Daly JW. Forskolin: unique diterpene activator of adenylate cyclase in membranes and in intact cells. Proc Natl Acad Sci U S A 1981;78(6):3363–7.
[47] Leavens KF, Birnbaum MJ. Insulin signaling to hepatic lipid metabolism in health and disease. Crit Rev Biochem Mol Biol 2011;46(3):200–15.
[48] Galsgaard KD, Pedersen J, Knop FK, Holst JJ, Wewer Albrechtsen NJ. Glucagon receptor signaling and lipid metabolism. Front Physiol 2019;10:413.
[49] Ling AV, Gearing ME, Semova I, Shin DJ, Clements R, Lai ZW, et al. FoxO1 is required for most of the metabolic and hormonal perturbations produced by hepatic insulin receptor deletion in male mice. Endocrinology 2018;159(3):1253–63.
[50] Stohr O, Tao R, Miao J, Copps KD, White MF. FoxO1 suppresses Fgf21 during hepatic insulin resistance to impair peripheral glucose utilization and acute cold tolerance. Cell Rep 2021;34(12):108893.
[51] Sostre-Colon J, Gavin MJ, Santoleri D, Titchenell PM. Acute deletion of the FOXO1-dependent hepatokine FGF21 does not alter basal glucose homeostasis or lipolysis in mice. Endocrinology 2022;163(5).
[52] Reily C, Stewart TJ, Renfrow MB, Novak J. Glycosylation in health and disease. Nat Rev Nephrol 2019;15(6):346–66.
[53] Fujita-Yamaguchi Y, Sato Y, Kathuria S. Removal of sialic acids from the purified insulin receptor results in enhanced insulin-binding and kinase activities. Biochem Biophys Res Commun 1985;129(3):739–45.
[54] Salhanick AI, Amatruda JM. Role of sialic acid in insulin action and the insulin resistance of diabetes mellitus. Am J Physiol 1988;255(2 Pt 1):E173–9.
[55] Fougerat A, Pan X, Smutova V, Heveker N, Cairo CW, Issad T, et al. Neuraminidase 1 activates insulin receptor and reverses insulin resistance in obese mice. Mol Metab 2018;12:76–88.
[56] Uehara K, Santoleri D, Whitlock AEG, Titchenell PM. Insulin regulation of hepatic lipid homeostasis. Compr Physiol 2023;13(3):4785–809.
[57] Markan KR, Naber MC, Ameka MK, Anderegg MD, Mangelsdorf DJ, Kliewer SA, et al. Circulating FGF21 is liver derived and enhances glucose uptake during refeeding and overfeeding. Diabetes 2014;63(12):4057–63.
[58] Camporez JP, Jornayvaz FR, Petersen MC, Pesta D, Guigni BA, Serr J, et al. Cellular mechanisms by which FGF21 improves insulin sensitivity in male mice. Endocrinology 2013;154(9):3099–109.
[59] Jaiswal N, Gavin MG, Quinn 3rd WJ, Luongo TS, Gelfer RG, Baur JA, et al. The role of skeletal muscle Akt in the regulation of muscle mass and glucose homeostasis. Mol Metab 2019;28:1–13.
[60] Sasako T, Umehara T, Soeda K, Kaneko K, Suzuki M, Kobayashi N, et al. Deletion of skeletal muscle Akt1/2 causes osteosarcopenia and reduces lifespan in mice. Nat Commun 2022;13(1):5655.

[61] Lai YC, Liu Y, Jacobs R, Rider MH. A novel PKB/Akt inhibitor, MK-2206, effectively inhibits insulin-stimulated glucose metabolism and protein synthesis in isolated rat skeletal muscle. Biochem J 2012;447(1):137—47.
[62] Small L, Brandon AE, Parker BL, Deshpande V, Samsudeen AF, Kowalski GM, et al. Reduced insulin action in muscle of high fat diet rats over the diurnal cycle is not associated with defective insulin signaling. Mol Metab 2019;25:107—18.
[63] Marette A, Liu Y, Sweeney G. Skeletal muscle glucose metabolism and inflammation in the development of the metabolic syndrome. Rev Endocr Metab Disord 2014;15(4):299—305.
[64] Dotz V, Lemmers RFH, Reiding KR, Hipgrave Ederveen AL, Lieverse AG, Mulder MT, et al. Plasma protein N-glycan signatures of type 2 diabetes. Biochim Biophys Acta Gen Subj 2018;1862(12):2613—22.
[65] Adua E, Memarian E, Russell A, Trbojevic-Akmacic I, Gudelj I, Juric J, et al. High throughput profiling of whole plasma N-glycans in type II diabetes mellitus patients and healthy individuals: a perspective from a Ghanaian population. Arch Biochem Biophys 2019;661:10—21.
[66] Keser T, Gornik I, Vuckovic F, Selak N, Pavic T, Lukic E, et al. Increased plasma N-glycome complexity is associated with higher risk of type 2 diabetes. Diabetologia 2017;60(12):2352—60.
[67] Bansal P, Bansal P, Verma R. Association of serum sialic acid concentration with diabetic complications and cardiovascular risk factors in an Indian population. Arch Med Sci Atheroscler Dis 2021;6:e14—7.
[68] Ekin S, Meral I, Gunduz H, Mert N. Comparative study of total protein, and total and lipid-associated serum sialic acid levels in patients with type 2 diabetes mellitus. J Clin Lab Anal 2003;17(4):124—6.
[69] Englyst NA, Crook MA, Lumb P, Stears AJ, Masding MG, Wootton SA, et al. Percentage of body fat and plasma glucose predict plasma sialic acid concentration in type 2 diabetes mellitus. Metabolism 2006;55(9):1165—70.
[70] Gavella M, Lipovac V, Car A, Vucic M, Sokolic L, Rakos R. Serum sialic acid in subjects with impaired glucose tolerance and in newly diagnosed type 2 diabetic patients. Acta Diabetol 2003;40(2):95—100.
[71] Ibrahim MA, Abdulkadir A, Onojah A, Sani L, Adamu A, Abdullahi H. Modulation of sialic acid levels among some organs during insulin resistance or hyperglycemic states. Mol Cell Biochem 2016;411(1—2):235—9.
[72] Khalili P, Sundstrom J, Jendle J, Lundin F, Jungner I, Nilsson PM. Sialic acid and incidence of hospitalization for diabetes and its complications during 40-years of follow-up in a large cohort: the Varmland survey. Prim Care Diabetes 2014;8(4):352—7.
[73] Scheen AJ, Paquot N, Lefebvre PJ. Investigational glucagon receptor antagonists in Phase I and II clinical trials for diabetes. Expert Opin Investig Drugs 2017;26(12):1373—89.
[74] Guzman CB, Zhang XM, Liu R, Regev A, Shankar S, Garhyan P, et al. Treatment with LY2409021, a glucagon receptor antagonist, increases liver fat in patients with type 2 diabetes. Diabetes Obes Metab 2017;19(11):1521—8.

